INDOOR PROPAGATION MODEL FOR OFFICE ENVIRONMENT AT 900 MHZ AND 1800 MHZ

by

Mehmet Akif Erol

B.S., Electrical and Electronics Engineering, Boğaziçi University, 2012

Submitted to the Institute for Graduate Studies in
Science and Engineering in partial fulfillment of
the requirements for the degree of
Master of Science

Graduate Program in Electrical and Electronics Engineering
Boğaziçi University

2015

ACKNOWLEDGEMENTS

Foremost, I would like to thank my advisor Prof. Selim Şeker for his continuous support, guidance and immense knowledge. His advice together with undergradute and graduate courses I have taken from him was the biggest help to me in this thesis.

I thank my manager Banu Yurt Koç for her encouragement and tolerance. I thank NETAS Defense Department for providing me the technical equipment used in this dissertation. I would also like to thank my colleague İlker Kaya for his technical assistance with measurement setup.

I thank Reza Ashrafi for his help with MATLAB simulations.

I am deeply grateful to Gizem Özer for spending countless hours on helping this thesis. Completing this work would have been all the more difficult without moral and material support of her.

Last but not least, I would like to thank my family for their eternal love and encouragement in my life. Without their support, I wouldn't be at this point.

This research has been supported by NETAS.

ABSTRACT

INDOOR PROPAGATION MODEL FOR OFFICE ENVIRONMENT AT 900 MHZ AND 1800 MHZ

Propagation of electromagnetic waves became an important area of research since the invention of wireless communication. Propagation models are generally divided into three categories. First category includes terrestrial and satellite link communication channel. This propagation environment is characterized by very long range, atmospheric effects and generally LOS propagation. Second category includes macrocells which are generally regarded as primary communication hubs of GSM network. Macrocell propagation environment is associated with street canyons, tall buildings, hills and trees. Third and last category includes picocells which are base stations located inside buildings. Indoor propagation environment presented new challenges such as multi-wall penetration, diffraction through corners and reflection from the walls. During the last decade, the necessity of using the same bandwidth for as many custormers as possible began to force GSM providers to deploy more and more picocells into indoor environments. This development increased the importance of precise and easy-to-use propagation models. Several empirical and theoretical propagation models for indoor propagation were proposed by various researchers. However, unlike macrocell models, none of those models seem to be de facto norm for quick propagation assesment and they generally produce varying results. In this dissertation, existing indoor propagation models were applied to a typical office building environment at two main GSM frequencies, comparison and accuracy of different models were presented and finally an optimized model adjusted specifically to an office environment was proposed using previous work as a base.

ÖZET

OFİS ORTAMLARI İÇİN 900 MHZ ve 1800 MHZ'DE KAPALI ORTAM YAYILIM MODELİ

Kablosuz haberleşmenin icadından bu yana elektromanyetik dalgaların yayılımı önemli bir araştırma alanı haline gelmiştir. Yayılım modelleri genellikle üç kategoriye ayrılırlar. İlk kategori karasal ve uydu sabit linkleri içermektedir. Bu yayılım ortamı uzun mesafe, atmosferik etkiler ve genellikle LOS yayılımı ile karakterize edilir. İkinci kategori GSM ağının genellikle başlıca iletişim merkezi olarak görülen makrohücrelerdir. Makrohücre ortamı caddeler, yüksek binalar, tepeler ve ağaçlar ile ilintilidir. Üçüncü ve son kategori ise kapalı ortamlara yerleştirilen pikohücrelerdir. Kapalı ortamlardaki yayılım birden fazla sayıda duvar penetrasyonu, köşelerden kırılma ve insan sayısının etkisi gibi yeni zorluklar eklemiştir. Son on yılda aynı frekans bandını olabildiğince çok müşteri için kullanma zorunluluğu GSM operatörlerini gittikçe daha fazla sayıda pikohücreyi kapalı ortamlara yerleştirmeye zorlamıştır. Bu durum hassas ve kolay yayılım modellerinin önemini artırmıştır. Çeşitli araştırmacılar tarafından kapalı ortamlar için empirik ve teorik yayılım modelleri önerilmiştir. Fakat makrohücre modellerinin aksine bu modellerden hiçbirisi hızlı bir yayılım değerlendirmesi için bir fiili standard olamamış gözükmektedir ve de bu modeller genellikle birbirlerinden oldukça farklı sonuçlar üretmektedir. Bu çalışmada varolan kapalı ortam yayılım modelleri tipik bir ofis binasına iki ana GSM frekansında uygunlanmış, bu modellerin kıyaslaması ve hassasiyeti sunulmuş ve son olarak da önceki çalışmalar kullanılarak özellikle ofis ortamları için optimize edilmiş bir model önerilmiştir.

TABLE OF CONTENTS

LIST OF FIGURES

LIST OF TABLES

LIST OF SYMBOLS

d	Distance
D	Diffraction parameter
E	Electric field
f	Frequency
G_R	Receiver antenna gain
G_T	Transmitter antenna gain
k	Wavenumber
L	Path loss
P_R	Received power
P_T	Transmitted power
$R_\parallel$	Reflection coefficient for horizontally polarized field
$R_\perp$	Reflection coefficient for vertically polarized field
$T_\parallel$	Transmission coefficient for horizontally polarized field
$T_\perp$	Transmission coefficient for vertically polarized field
Z	Impedance of a medium
α	Attenuation constant
ϵ	Permittivity of a material
θ	Angle of incidence
λ	Wavelength
μ	Permeability of a material
σ	Conductivity of a material
υ	Fresnel parameter

LIST OF ACRONYMS/ABBREVIATIONS

BSC	Base Station Controller
BST	Base Station Tower
EHF	Extremely High Frequency
GSM	Global System for Mobile Communication
ITU-R	International Telecommunication Union Radio Communication Sector
LNA	Low Noise Amplifier
LOS	Line-of-Sight
MS	Mobile Station
MSC	Mobile Switching Center
NLOS	Non-Line-of-Sight
PSTN	Public Switched Telephone Network
SHF	Super High Frequency
SMRE	Square Means Relative Error
UHF	Ultra High Frequency
UTD	Uniform Theory of Diffraction
VHF	Very High Frequency
WLAN	Wireless Local Area Network

1. INTRODUCTION

Telecommunication which is defined as communication at a distance by electrical wires or electromagnetic waves is one of the foundations of modern civilization. Global economy requires instant communication between one part of the world to another. During Cold War, both USA and USSR were capable of launching missiles within minutes. This frightening speed necessiated the same speed of communication. Our daily life was also profoundly affected by modern technology. Instant access to information enabled us to quickly determine our decisions.

1.1. History of Telecommunications

History of modern telecommunications starts with the invention of electrical telegraphy. Telegraph uses electrical signals over a wire to achieve a point-to-point communication. Telegraphy revolutionized communication during nineteenth century. Speed of electrical signals reduced transatlantic communication from several days to a matter of minutes. Telegraph was followed by telephone networks. Telephone networks used same wired electrical communication principle as telegraphs. Their main difference was that telegraph required knowledge of Morse code as it sent the message in simple ON-OFF form while telephone required no special knowledge. Submarine cables were installed connecting most of the globe to each other. Early cables had both electrical and bandwidth problems. Introduction of fiber-optic cables dramatically increased useable bandwidth. Much later on, these "telephone" cables became massive data transmission hubs for internet.

While telegraphy and telephony were beginning of modern telecommunications, introduction of electromagnetic waves for communication truly revolutionized it. Radio was invented by Marconi in 1891 and was commercialized rapidly. A model for a radio transmission system is given in Figure 1.1. Classical radio transmission system included modulation and demodulation of electromagnetic waves using some kind of electronic hardware. With the rise of semiconductor electronics after World War II,

more advanced wireless communication devices began to enter daily lives. Television technology which was just another form of radio, has long been known but its rapid expansion happened with scientific breakthroughs in bandwidth use and electronic hardware.

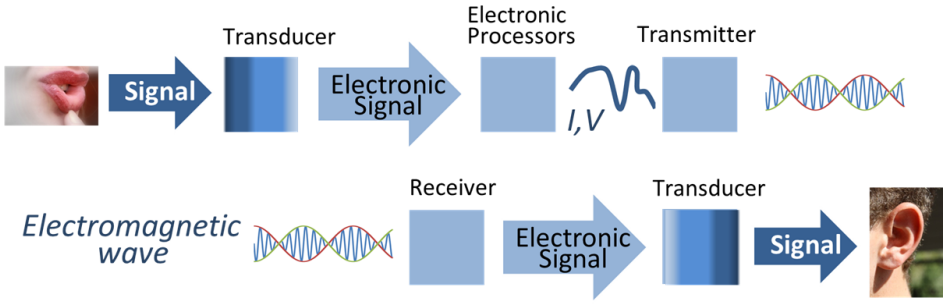

Figure 1.1. Radio Transmission System.

Introduction of satellites into telecommunications started with the launch of Soviet satellite *Sputnik* into space in 1957. This development fostered the research on satellite communications. Today, communication satellites are mainly used to transmit TV broadcasts. Another application of communication satellites is satellite telephony. Long distance telephony systems were implemented using satellites in places where there were not any submarine cables. In such systems, the uplink would first connect to his local PSTN network and his call would be forwarded to an earth station and then to communication satellite. The downlink also follows an analogous path. Satellites have very large coverage. While this was good in terms of accessability, it severely limited the maximum number of users for satellite phones due to limited bandwidth. High cost of satellites and satellite receiver-transmitter stations connected to PSTN networks ultimately confined satellite telephony to limited number of people at very high prices for vital communications.

Although television or radio are examples of wireless communication in scientific terms, we do not think them as "wireless communication" as what we understand from wireless communication today is bidirectional data transfer through electromagnetic waves. Utilization of bidirectional wireless transmission started with radiotelephony in 1940s. These devices operated at radio frequencies and were generally connected to

local PSTN network. Problem of these early systems was that bandwidth requirement was too high due to problems with mass producing tight RF filters, LNA and receiver amplifiers. High power transmitters were used in radiotelephone systems and these required vast distances for reuse of same frequencies. These resulted in heavy congestion in radiotelephony networks and limited capacity was mainly reserved for emergency purposes. Another problem was that these portable devices were too heavy to carry with [1].

In 1970s, further electronic development enabled enough device miniaturization to manufacture truly portable mobile wireless communication devices. Concept of cellular network that was proposed in 1947 by Bell Labaratory solved the problems of early radiotelephone systems. Swedish company Ericsson first implemented digital switching system that combines cellular network into a single network. Although switching was digital, transmission was still analog [1].

In 1980s, the development was drifting towards digital transmission as analog systems had very bad spectral efficiency. As number of customers increased dramatically, the service providers needed a system that would benefit from bandwidth more efficiently. Digital phones turned cellular communications, which were already on the road to success, into a blockbuster. Digital communication standards like GSM were developed to set a standard and were quickly accepted by users due to superior service quality of digital transmission over analog one [2].

From 2000s onwards, investment in wireless communication soars up due to three factors; increasing range of products, increasing data transmission for products and higher numbers of new customers. These three factors are forcing academic research to find better solutions to problems of wireless communication.

1.2. Challenges in Wireless Communication

Main challenges in wireless communication could be summarized as follows:

- Multipath propagation: i.e., the fact that a transmit signal can reach the receiver via different paths (e.g., reflections from different houses or mountains).
- Spectrum limitations.
- Energy limitations.
- User Mobility [3].

1.3. Cellular Network

Cellular networks are called such because they divide geographical regions into communication cells. The reason behind dividing regions into cells is to use the same frequencies as many times as possible; thus solving "Spectrum Limitations" problem. Each cell contains its own fixed-location transceiver (usually called base station). Neighboring cells use different frequencies to prevent interference. As areas are reduced by cells, power of both transmitter and receiver are reduced as well.

Hexagonal cells became conventional throughout the world. Typical cellular network is shown in Figure 1.2. In this example, MS connects to BST in its hexagonal cell. Multiple BSTs communicate with a BSC. Network traffic measurement, authentication and handover management are some functions of BSC. Finally, all BSCs are connected to MSC with a microwave link or telephone cables. MSC is where calls are routed. MSC also connects to PSTN for communication with land-based telephones and other mobile stations.

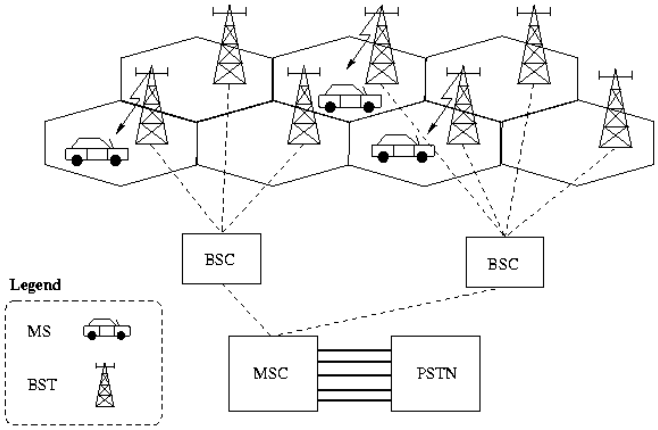

Figure 1.2. Cellular Network Example.

Main concern in mobile communications is to use limited bandwidth most effectively. The demand for bandwidth increased dramatically over the last decade and it is expected to increase at an accelerated pace in the future. Data traffic caused by cell phones, PDAs and other mobile devices forces mobile service providers to reduce cell sizes for reusing same frequency band for as many customers as possible. This means smaller and smaller cell areas. These cell areas are now as small as a single house.

1.4. Wireless Propagation Channel

Wireless propagation channel places fundamental limitations on the performance of wireless communication systems. The transmission path between the transmitter and the receiver can vary from simple LOS to one that is severely obstructed by buildings, mountains and foliage. Unlike wired channels that are stationary and predictable, wireless channels are extremely random and do not offer easy analysis. Even the speed of motion impacts how rapidly the signal level fades as a mobile terminal moves in space. Modeling the wireless channel has historically been one of the most difficult part of wireless system design [2].

The wireless channel representation is shown in Figure 1.3. Estimation of channel noise is the primary aim needed for a stable wireless communication system. Channel noise can be subdivided into multiplicative and additive effects. The additive noise arises from the noise generated within the receiver itself, such as thermal and shot noise in passive and active components and also from external sources such as atmospheric effects, cosmic radiation and interference from other transmitters and electrical appliances [4]. The multiplicative noise arises from the various processes encountered by transmitted waves on their way from the transmitter antenna to the receiver antenna. Some of them are listed below:

- The directional characteristics of both the transmitter and receiver antennas.
- Reflection (from the smooth surfaces of walls and hills).
- Absorption (by walls, trees and by the atmosphere).
- Scattering (from rough surfaces such as the sea, rough ground and the leaves and

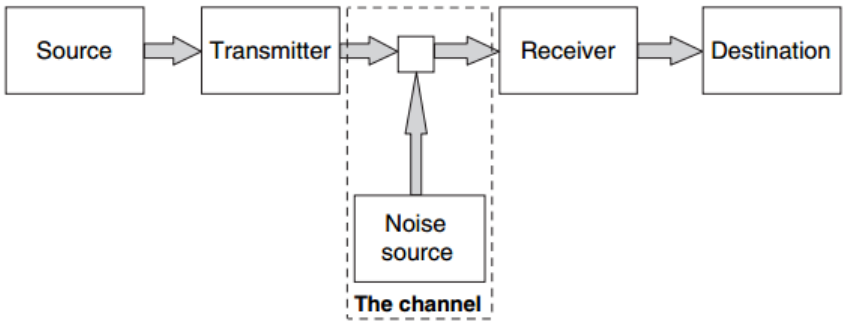

Figure 1.3. Wireless Channel Representation.

branches of trees).

- Diffraction (from edges, such as building rooftops and hilltops).
- Refraction (due to atmospheric layers and layered or graded materials).

It is conventional to further subdivide the multiplicative processes in the channel into three types of fading: *path loss, shadowing* (or *slow fading)* and *fast fading* (or *multipath fading*), which appear as time-varying processes between the antennas, as shown in Figure 1.4 [4].

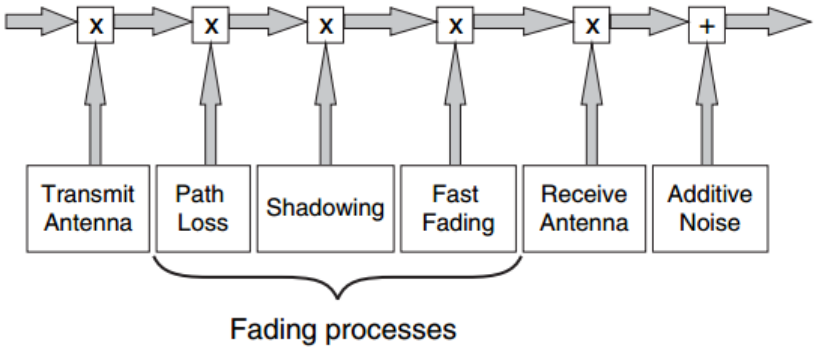

Figure 1.4. Multiplicative Noises for the Wireless Channel.

1.4.1. Free Space Loss

Free space loss is defined as the loss in signal strength of an electromagnetic wave that would result from LOS path through space. Friis equation is used to estimate

receiver power at some distance away from transmitter. It is given by,

$$P_R = P_T G_T G_R (\frac{\lambda}{4\pi r})^2, \tag{1.1}$$

where r is distance between transmitter and receiver and $(\frac{\lambda}{4\pi r})^2$ is *free space loss loss factor*.

According to Friis equation, it seems that as frequency increases, the received power decreases. This contradiction is caused by the assumption that receiver antenna gain to be independent of frequency. If we assume G_R to be function of frequency, then dependence on frequency would be no more. Friis equation is valid only far-field region of the antenna. Far-field distance of antenna is known as *Rayleigh Distance* and is given by,

$$d_R = (\frac{2L_a^2}{\lambda}), \tag{1.2}$$

where L_a is the largest dimension of the antenna.

Friis law received power for free space in units of dB is given by,

$$P_{R|dBm} = P_{T|dBm} + G_{T|dB} + G_{R|dB} + 20\log(\frac{\lambda}{4\pi r}). \tag{1.3}$$

Taking free space loss as $L_{F|dB} = P_{T|dBm} + G_{T|dB} + G_{R|dB} - P_{R|dBm}$, the equation could be further simplified as follows,

$$L_{F|dB} = 32.4 + 20\log r + 20\log f, \tag{1.4}$$

Where r is in kilometers and f is in megahertz.

In order to better point out distance dependence of the equation, we generally

first calculate path loss at 1-m distance and then express the equation as follows [3],

$$L_{F|dB}(d) = L_{0|dB}(1m) + 20\log(d). \tag{1.5}$$

1.4.2. Reflection

In practical situations, radio waves will reflect off walls and off the ground. In mobile communications within cities, reflections off such surfaces often form the major propagation mechanism. When a radio wave reflects off a surface, the strength of the reflected wave is less than that of the incident wave. The ratio of the two is known as the "reflection coefficient" of the surface. This depends upon the conductivity and permittivity of the material that forms the reflective surface, as well as its thickness and the frequency, angle of incidence and polarisation of the incident wave. Good conductors are near-perfect reflectors of electromagnetic waves at frequencies used for radio communications. Dielectrics, such as glass, are less good reflectors, as are walls made of brick or concrete. Geometry for calculating the reflection coefficients are shown in Figure 1.5 [5].

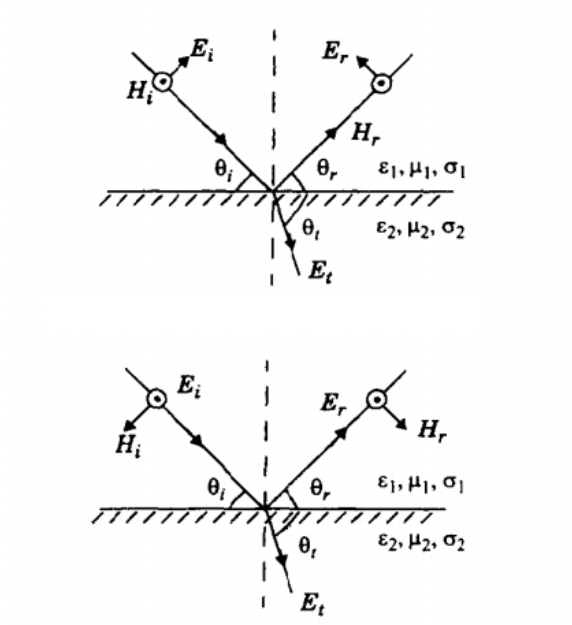

Figure 1.5. Geometry of reflection.

The impedance of a media is given by,

$$Z = \sqrt{\frac{\mu}{\epsilon}}. \tag{1.6}$$

Reflection and transmission coefficients at the boundary is then derived from Maxwell equations as follows,

$$R_{\parallel} = \frac{Z_1 \cos\theta_i - Z_2 \cos\theta_t}{Z_2 \cos\theta_t + Z_1 \cos\theta_i}, \qquad R_{\perp} = \frac{Z_2 \cos\theta_i - Z_1 \cos\theta_t}{Z_2 \cos\theta_i + Z_1 \cos\theta_t}. \tag{1.7}$$

$$T_{\parallel} = \frac{2Z_2 \cos\theta_i}{Z_2 \cos\theta_t + Z_1 \cos\theta_i}, \qquad T_{\perp} = \frac{2Z_2 \cos\theta_i}{Z_2 \cos\theta_i + Z_1 \cos\theta_t}. \tag{1.8}$$

1.4.3. Diffraction

Diffraction occurs when the radio path between the transmitter and receiver is obstructed by a surface that has sharp edges. The secondary waves resulting from the obstructing surface are present throughout the space and even behind the obstacle, giving rise to a bending of waves around the obstacle, even when LOS path does not exist between transmitter and receiver. At high frequencies, diffraction, like reflection, depends on the geometry of the object, as well as the amplitude, phase and polarization of the incident wave at the point of diffraction.

Estimating the signal attenuation caused by diffraction of radio waves over hills and buildings is essential in predicting the field strength in a given service area. Generally, it is impossible to make very precise estimates of the diffraction losses, and in practice prediction is a process of theoretical approximation modified by necessary empirical corrections. Though the calculation of diffraction losses over complex and irregular terrain is a mathematically difficult problem, expressions for diffraction losses for many simple cases have been derived. As a starting point, the limiting case of prop-

agation over a knife-edge gives good insight into the order of diffraction loss. Diffraction parameters for knife-edge obstruction are shown in Figure 1.6 [2].

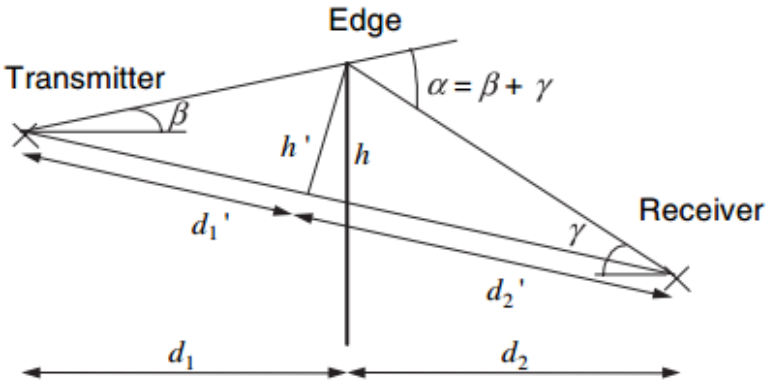

Figure 1.6. Knife-edge diffraction parameters.

Now, *diffraction parameter,*v could be approximated as,

$$v \approx h\sqrt{\frac{2(d_1 + d_2)}{\lambda d_1 d_2}}. \tag{1.9}$$

Propagation loss due to knife-edge diffraction could be found using Fresnel integrals. Good approximation of these integrals for $v > 1$ (well within the shadow region) is given by,

$$L_{ke} \approx -20 \log \frac{1}{\pi v \sqrt{2}} \approx -20 \log \frac{0.225}{v}. \tag{1.10}$$

Variation of L_{ke} with v is shown in Figure 1.7.

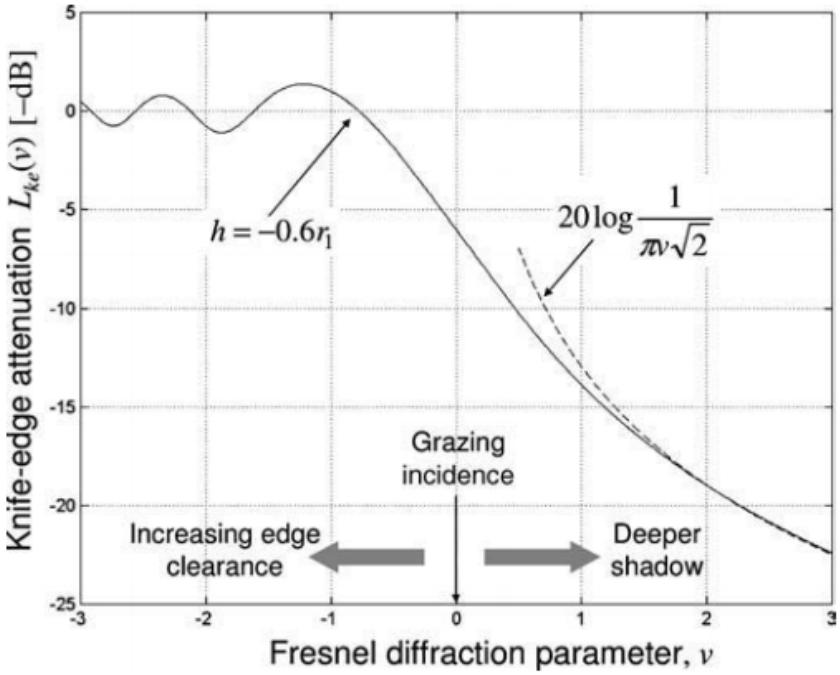

Figure 1.7. Knife-edge diffraction loss.

Useful way of understanding the concept of diffraction is *Fresnel Zones*. Fresnel zones around knife-edge obstruction are shown in Figure 1.8. r_n denotes *Fresnel zone radius*.

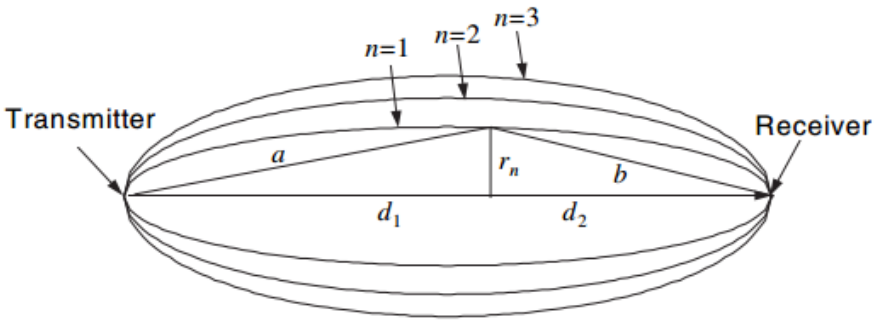

Figure 1.8. Fresnel Zones.

If we assume that $r_n \ll d_1$ and $r_n \ll d_2$, good approximation of *Fresnel zone radius* is given by,

$$r_n \approx \sqrt{\frac{n\lambda d_1 d_2}{d_1 + d_2}}. \tag{1.11}$$

The Fresnel zones can be thought of as containing the main propagating energy in the wave. Contributions within the first zone are all in phase, so any absorbing obstructions which do not enter this zone will have little effect on the received signal. The *Fresnel zone clearance* (h/r_n) can be expressed in terms of the diffraction parameter v as follows [4],

$$v \approx \frac{h}{r_n}\sqrt{2n}. \tag{1.12}$$

When the obstruction occupies 0.6 times the first Fresnel zone, the v parameter is then approximately -0.8. Referring to Figure 1.7, the obstruction loss is then 0 dB. This clearance is often used as a criterion to decide whether an object is to be treated as a significant obstruction [4].

1.4.4. Absorption

The section 1.4.2 provided basic transmission and reflection coefficients for electromagnetic propagation. Transmission coefficients given in Equation 1.7 and Equation 1.8 are valid in a dielectric halfspace. These equations are important for ground reflections and reflections by terrain features. *Transmission through* a dielectric layer occurs when a transmitter and a receiver are seperated by brick or concrete wall. In that case, we are interested in the attenuation and phase shift of a wave transmitted through a wall.

The basic problem of transmission and reflection through dielectric layers is detailed in [6]. The most practical situation occurs when a dielectric layer is surrounded by air from both sides. Transmission and reflection coefficients are determined as summation of partial waves. Transmission coefficient is given by [6],

$$T = \frac{T_1 T_2 e^{-j\alpha}}{1 + R_1 R_2 e^{-2j\alpha}}, \tag{1.13}$$

where α is the electrical length of the dielectric as seen by waves, T_1 is the transmission

coefficient of a wave from air into a dielectric halfspace and T_2 is the transmission coefficient from dielectric into air. Both T_1 and T_2 could be computed using the formulas in Section 1.4.2.

Reflection coefficient is given by [6],

$$R = \frac{R_1 + R_2 e^{-j2\alpha}}{1 + R_1 R_2 e^{-2j\alpha}}. \tag{1.14}$$

Finally α is given by,

$$\alpha = \frac{2\pi}{\lambda}\sqrt{\epsilon_{r,2}} d_{layer} \cos\theta_t, \tag{1.15}$$

where d_{layer} is the geometrical length of the layer.

We assumed wall as a lossless dielectric medium. However, in practice walls have finite conductivity. In order to find total loss of power along the wall, it is necessary to include *attenuation constant* into equation. A linearly polarized wave in x-direction could be written as [7],

$$\boldsymbol{E} = \boldsymbol{a_x} E_x. \tag{1.16}$$

E_x could be then written as,

$$E_x = E_0 e^{-\alpha z} e^{-j\beta z}, \tag{1.17}$$

where α is *attenuation constant* and β is *phase constant.*

So, we summarize the propagation along the wall as the through dielectric layer transmission plus absorption loss due to finite conductivity of wall. With the knowledge of attenuation constant and thickness of a wall, absorption loss factor could be added

to the equation.

1.5. Propagation Models

For the design, simulation, and planning of wireless systems, we need models for the propagation channels. There are two main applications for channel models [3]:

(i) For the design, testing, and type approval of *wireless systems*, we need simple channel models that reflect the important properties of propagation channels i.e., properties that have an impact on system performance. This is usually achieved by simplified channel models that describe the statistics of the impulse response in parametric form. The number of parameters is small and *independent of specific locations*. Such models sometimes lead to insights due to closed-form relationships between channel parameters and system performance. Furthermore, they can easily be implemented by system designers for testing purposes.

(ii) The designers of *wireless networks* are interested in optimizing a given system in a certain geographical region. Locations of Base Stations(BSs) and other network design parameters should be optimized on the computer, and not by field tests, and trial and error. For such applications, *location-specific channel models* that make good use of available geographical and morphological information are desirable. However, the models should be robust with respect to small errors in geographical databases.

1.6. Types of Wireless Communication Systems

Six types of wireless communication system are shown in Figure 1.9 [4].

- *Satellite fixed links:* These are typically created between fixed earth stations with large dish antennas and geostationary earth-orbiting satellites. The propagation effects are largely due to the Earths atmosphere, including meteorological effects such as rain. Usually operated in the SHF and EHF bands.
- *Terrestrial fixed links:* Used for creating high data rate links between points on

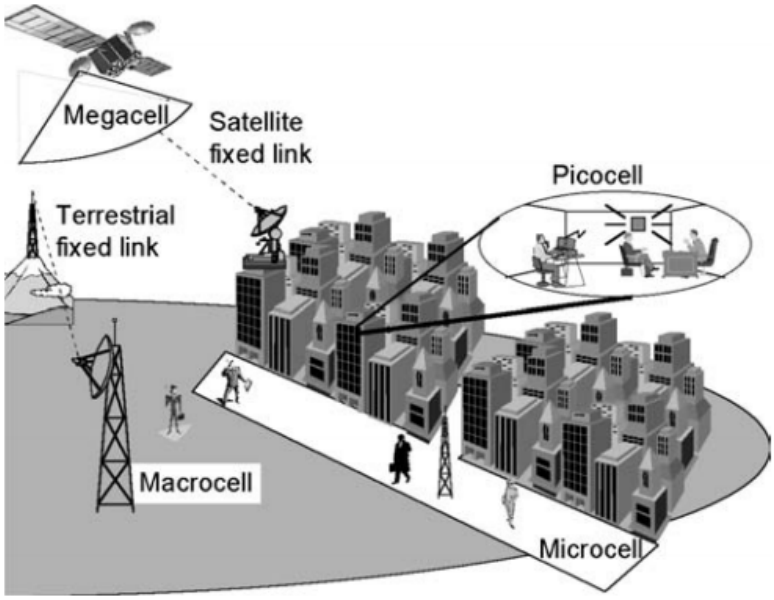

Figure 1.9. Wireless communication system types.

the Earth, for services such as telephone and data networks, plus interconnections between base stations in cellular systems. Also used for covering wide areas in urban and suburban environments for telephone and data services to residential and commercial buildings. Meteorological effects are again significant, together with the obstructing effects of hills, trees and buildings. Frequencies from VHF through to EHF are common.

- *Megacells:* These are provided by satellite systems (or by high-altitude platforms such as stratospheric balloons) to mobile users, allowing coverage of very wide areas with reasonably low user densities. A single satellite in a low earth orbit would typically cover a region of 1000 km in diameter. The propagation effects are dominated by objects close to the user, but atmospheric effects also play a role at higher frequencies.
- *Macrocells:* Designed to provide mobile and broadcast services (including both voice and data), particularly outdoors, to rural, suburban and urban environments with medium traffic densities. Base station antenna heights are greater than the surrounding buildings, providing a cell radius from around 1 km to many tens of kilometres. Mostly operated at VHF and UHF.
- *Microcells:* Designed for high traffic densities in urban and suburban areas to

users both outdoors and within buildings. Base station antennas are lower than nearby building rooftops, so coverage area is defined by street layout. Cell length up to around 500 m. Again mostly operated at VHF and UHF, but services as high as 60 GHz have been studied.

- *Picocells:* Very high traffic density or high data rate applications in indoor environments. Users may be both mobile and fixed; fixed users are exemplified by wireless local area networks between computers. Coverage is defined by the shape and characteristics of rooms, and service quality is dictated by the presence of furniture and people.

1.7. Thesis Outline

In the first section, challenges of wireless communication, cellular network concept, fundamental wireless propagation modes, the need for propagation models and wireless communication system types are explained. This thesis focuses on developing a propagation model for a modern office building at microwave frequencies. The aim is to develop accurate propagation loss model for indoor base stations and WLAN access points. For this purpose, a configurable base station is used as *picocell* in NETAS Main Office at Kurtkoy, Istanbul.

Chapter 2 provides existing picocell indoor propagation models in the literature and their experimental results. Dominant mode of propagation and contribution of each different mode for these models are analyzed.

First part of Chapter 3 explains measurement procedure and relevant information. Floor maps of NETAS Main Office are used to mark location and details of each measurement. In the second part of Chapter 3, measured path losses are compared to predicted path losses of each model. Results are evaluated to show strengths and weaknesses of the models. Final secion of Chapter 3 includes brief comparison of picocell indoor propagation models.

In Chapter 4, an optimized propagation model is proposed by taking different

contributions from existing picocell models and adjusting model parameters for office environment. New formula and parameters for optimized model are presented and finally results and comparisons are included.

The last chapter addresses several concluding remarks and some areas and suggestions for possible future works are also included.

2. INDOOR PROPAGATION MODELS FOR PICOCELL

In this chapter, propagation loss models for picocells in the literature are explained in detail. Models described in this section are implemented in our test environment in Chapter 4.

2.1. Single-Slope Model

Single-slope model is the simplest way to characterize path loss for indoor propagation. Single-slope model modifies free path loss exponent of 20 to account for various other losses stemming from diffraction, reflection, absorption, etc. The basic equation is modified version of Equation 1.5 and is given by,

$$L(d) = L_0(1m) + N\log(d), \tag{2.1}$$

where N is specific path loss exponent and d is distance between transmitter and receiver.

Although Single-slope model gives good approximation for *macrocell* and *microcell* systems, it tends to give excessive errors for *picocells* because of the large variability in propagation mechanisms among different building types and among different paths within a single building. L_0 and N values for single-slope model at 1800 MHz were provided in [8] and shown in Table 2.1. For 900 MHz, modification of L_0 by 10 dB for multi-floor case and 8 dB for single-floor case was proposed in [9]. Same path loss exponent value is proposed for 900 MHz.

2.2. Dual-Slope Model

Dual-Slope model, as the name itself implies, has two slopes; the first is for LOS and the second is for NLOS region. As Single-slope model is not enough to model propagation in the intermediate near zone region, another slope was added. This new

Table 2.1. Coefficients for Single-Slope model at 1800 MHz.

Environment	$L_0[dB]$	N
Dense		
one floor	33.3	40
two floors	21.9	52
multi floor	44.9	54
Open	42.7	19
Large	37.5	20
Corridor	39.2	14

slope was meant to provide smooth transition for *Fresnel breakpoint*. The equation for the model is provided in Equation 2.2 [10],

$$L = L_0 + \begin{cases} N_1 \log_{10} d & 1m < d \leq d_{bp}, \\ N_1 \log_{10} d_{bp} + N_2 \log_{10}(\frac{d}{d_{bp}}) & d > d_{bp}, \end{cases} \tag{2.2}$$

where N_1 is path loss exponent for LOS region, N_2 is path loss exponent for NLOS region and d_{bp} is break-point distance.

Break-point distance d_{bp} is a site-specific parameter which is chosen as the distance where LOS to NLOS transition happens. $N_1 = 2$ is generally used for the region prior to *Fresnel breakpoint*. There is much more variability in the path loss for the region beyond the *Fresnel breakpoint*, with values of N_2 ranging from 20 to 70 [11].

2.3. Log-Normal Shadowing Model

The log-normal distribution describes the random shadowing effects which occur over a large number of measurement locations which have the same T-R seperation, but have different levels of clutter on the propagation path. This phenomenon is referred to as *log-normal shadowing*. Simply put, log-normal shadowing implies that

measured signal levels at a specific T-R seperation have a Gaussian distribution about the distance-dependent mean of Equation 2.1 where the measured signal levels have values in dB units. The standard deviation of the Gaussian distribution that describes the shadowing also has units in dB. The equation for the model is given by [2],

$$L(d) = L_0(1m) + N\log(d) + X_\sigma, \tag{2.3}$$

where X_σ is a zero-mean Gaussian distributed random variable with standard deviation σ.

Extensive measurements were conducted at 914 MHz by Seidel and Rappaport in [12] to determine parameters N and σ which are functions of building type, building wing and number of floors between transmitter and receiver. Results of these measurements are shown in Table 2.2.

Table 2.2. N and σ parameters for Log-Normal Shadowing Model.

Environment	N	σ
All Locations	31.4	16.3
Same floor	27.6	12.9
Through 1 Floor	41.9	5.1
Through 2 Floors	50.4	6.5
Through 3 Floors	52.2	6.7
Office Building I	35.4	12.8
Office Building II	43.3	13.3

2.4. ITU-R Model

An empirical loss model was suggested by ITU-R for indoor radio communication planning in [13]. In ITU-R model, distance losses are included implicitly by varying *path loss exponent* values. Penetration through multiple floors are also accounted explicitly.

The basic loss equation has the following form,

$$L_{total} = 20 \log f + N \log d + L_f(n) - 28, \tag{2.4}$$

where N is path loss exponent, f is frequency in MHz, d is distance between transmitter and receiver, L_f is floor penetration loss factor and n is number of floors between transmitter and receiver.

Free space path loss exponent of 20 is modified by ITU-R model to account for various other losses like diffraction, reflection, absorption by the walls etc. The model has also added a coefficient for floor penetration.

Path loss exponents for ITU-R model in various different environments and frequencies are given in Table 2.3 [13].

Table 2.3. Power loss exponents for ITU-R model.

Frequency	Residential	Office	Commercial
900 MHz	-	33	20
1.2-1.3 GHz	-	32	22
1.8-2.0 GHz	28	30	22
4 GHz	-	28	22
60 GHz	-	22	17

Floor penetration loss factors for ITU-R model are given in Table 2.4 [13].

Following general conclusions for ITU-R model are drawn in [13].

- Paths with a line-of-sight component are dominated by free space loss and have a distance power loss exponent of around 20.
- Large open rooms also have a distance power loss exponent of around 20; this may be due to a strong line-of-sight component to most areas of the room. Examples

Table 2.4. Floor penetration loss factors for ITU-R model.

Frequency	Residential	Office	Commercial
900 MHz	-	9 (1 floor) 19 (2 floors) 24 (3 floors)	-
1.8-2.0 GHz	$4n$	15+4(n-1)	6+3(n-1)

include rooms located in large retail stores, sports arenas, open-plan factories, and open-plan offices.

- Corridors exhibit path loss less than that of free space, with a typical distance power loss exponent of around 18. Grocery stores with their long, linear aisles exhibit the corridor loss characteristic.
- Propagation around obstacles and through walls adds considerably to the loss which can increase the power distance exponent to about 40 for a typical environment. Examples include paths between rooms in closed-plan office buildings.
- For long unobstructed paths, the first Fresnel zone breakpoint may occur. At this distance, the distance power loss exponent may change from about 20 to about 40.

2.5. Motley-Keenan Model

Motley and Keenan proposed an empirical indoor propagation model in [14]. In this model, path loss exponents at 900 MHz and 1700 MHz were determined by measurements. Furthermore, losses through floors and walls were included with additional loss factors with seperate loss factors for floor penetration and wall penetration. Motley-Keenan model has the following form,

$$L = L_1 + N \log r + n_f a_f + n_w a_w, \tag{2.5}$$

where L_1 is path loss at 1m, N is path loss exponent, n_f is number of floors, n_w is number of walls, a_f is attenuation factor per floor and a_w is attenuation factor per wall.

The equation above is the modified version of Equation 1.5. Path loss exponent of 20 in Equation 1.5 is modified by Motley-Keenan to accommodate extra losses of indoor propagation. Floor and wall penetration were also added explicitly with again empirical loss coefficients for floors and walls. N, L_1 and a_f values at 900 MHz and 1700 MHz are given in [14] and are shown in Table 2.5. However, no value for a_w is provided.

Table 2.5. Model parameters for Motley-Keenan model.

Parameter	900 MHz	1700 MHz
N	40	35
L_1	16	21
a_f	10	16

2.6. Improved Motley-Keenan Model

Improved version of Motley-Keenan model were proposed in [15] by Lima and Menezes. Improved model takes wall thickness into account to reduce predicton errors. The proposed adjustment to Motley-Keenan model is given as,

$$L = L_1 + N \log r + \sum k_i L w_i, \tag{2.6}$$

where k_i is number of type i walls and Lw_i is penetration loss coefficient for type i walls.

This model assumes the same penetration loss for each kind of wall type independent of its thickness. In order to introduce the thickness of each wall type, the

adjustment in Equation 2.7 was proposed [15].

$$L = L_1 + N \log r + \sum_{i=1}^{n} k_i L_{0i} 2^{\log_3 \frac{e_i}{e_{0i}}}, \tag{2.7}$$

where L_{0i} is the penetration loss in type i reference wall, e_{0i} is the thickness of type i reference wall and e_i is the thickness of type i wall which obstructs the signal.

Model in Equation 2.7 requires only the knowledge of the penetration loss in a reference wall built with a type i material and thickness e_{0i}. Reference penetration losses for three types of material were also provided in [15]. Table 2.6 shows these reference losses.

Table 2.6. Reference penetration losses for different types of materials.

Type of Wall	Thickness of the Wall (cm)	Penetration Loss (dB)
Soft Partition	5	2.5
Plasterboard	12	2.5
Concrete Wall	15	6

Authors of [15] conducted experiments for both standard Motley-Keenan model and their proposed improved model. Path loss values through different types of walls were measured and then compared to standard and improved models. The authors claim improvement of the square means relative error (SMRE) improvement from 5% to 3% percent. The results are shown in Figures 2.1 and 2.2 [15].

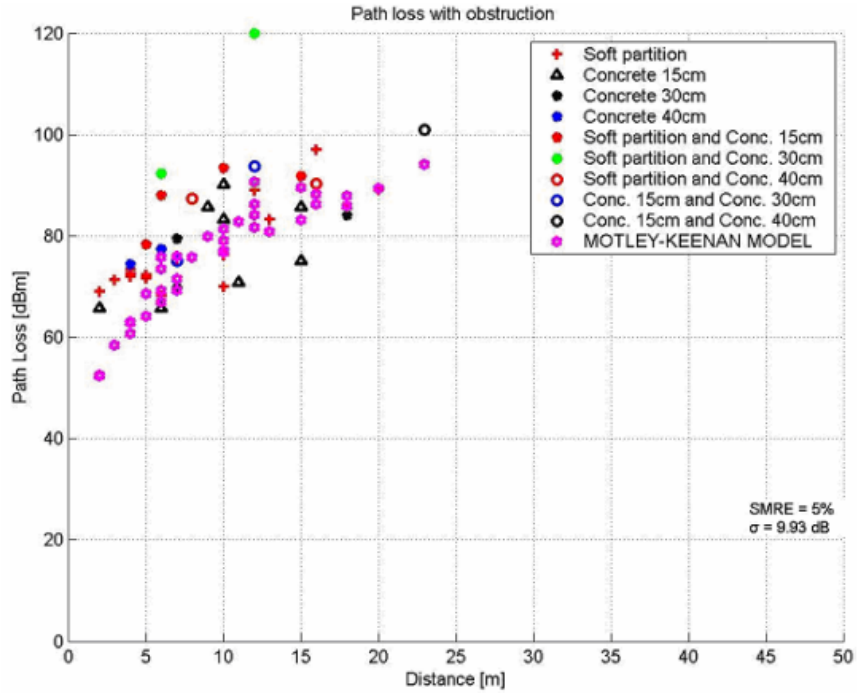

Figure 2.1. Motley-Keenan model with multiple wall obstructions.

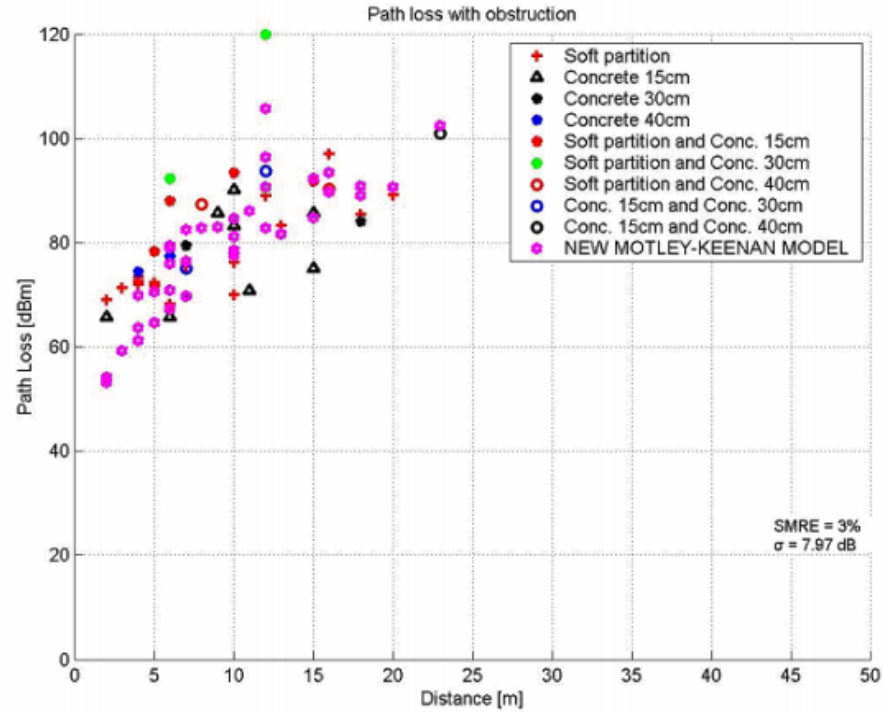

Figure 2.2. Improved Motley-Keenan model with multiple wall obstructions.

2.7. Akerberg Model

An empirical model was proposed by Akerberg in [16] for use at 900 MHz. The path loss including shadowing is considered to be a random variable, uniformly distributed between limits which vary with distance as indicated in Table 2.7.

Table 2.7. Upper and lower limits of path loss in Akerberg model.

Distance(m)	Lower limit of path loss(dB)	Upper limit of path loss(dB)
$1 \leq r < 10$	$30 + 20 \log r$	$30 + 40 \log r$
$10 \leq r < 20$	$20 + 30 \log r$	$40 + 30 \log r$
$20 \leq r < 30$	$-19 + 60 \log r$	$1 + 60 \log r$
$40 \leq r$	$-115 + 120 \log r$	$-95 + 120 \log r$

The path loss exponent increases from 20 to 120 as the distance increases. The model may be extended for use at 1800 MHz by the addition of 8.5 dB extra path loss at all distances [16].

2.8. Multi-Wall Model

The multi-wall model gives the path loss as the free space loss added with losses introduced by the walls and floors penetrated by the direct path between the transmitter and the receiver. It has been observed that the total floor loss is a non-linear function of the number of penetrated floors. This characteristic is taken into account by introducing an empirical factor b. The multi-wall model can then be expressed in form [8],

$$L = L_{FS} + L_C + \sum_{i=1}^{I} k_{wi} L_{wi} + k_f^{\left[\frac{k_f+2}{k_f+1} - b\right]} L_f, \tag{2.8}$$

where L_{FS} is free space loss between transmitter and receiver, L_C is contant loss, k_{wi} is number of penetrated walls of type i, k_f is number of penetrated floors, L_{wi} is loss

of wall type i, b is an empirical factor and I is number of wall types.

The constant loss in Equation 2.8 is a term which results when wall losses are determined from measurement results by using the multiple linear regression. Normally it is close to zero. The third term in Equation 2.8 expresses the total wall loss as a sum of the walls between transmitter and receiver. For practical reasons the number of different wall types must be kept low. Otherwise, the difference between the wall types would be small and their significance in the model would become unclear. A division into two wall types were proposed. These two wall types are shown in Table 2.8 [8].

Table 2.8. Wall types for the Multi-Wall model.

Wall Type	Description
Light Wall (L_{w1})	A wall that is not bearing load: e.g. plasterboard, particle board or thin ($< 10cm$), light concrete wall
Heavy Wall (L_{w2})	A load-bearing wall or other thick($> 10cm$) wall, made of e.g concrete or brick

Model coefficients for Multi-Wall model at 1800 MHz was provided in [8] and is given in Table 2.9.

Table 2.9. Model coefficients for the Multi-Wall model.

L_{w1}[dB]	L_{w2}[dB]	L_f[dB]	b
3.4	6.9	18.3	0.46

A difference of 1.5 dB in the light wall loss and a difference of 3.5 dB in the floor loss were suggested for 900 MHz in [8].

2.9. Multi-Wall-and-Floor Model

Motley-Keenan model takes into account all penetrated walls and floors by individual penetration losses depending on their thickness and material. Walls or floors of the same category (thickness and material) contribute a constant loss whether other walls or floors have been penetrated before or not. However, measurements and ray tracing simulations indicate a nonlinear dependence of the overall penetration loss and the number of penetrated floors of the same category. Multi-Wall model in Section 2.8 introduces an empirical exponent that contains the number of penetrated floors. Similar to the attenuation owing to traversed floors, it has been found that the attenuation caused by the first traversed wall is greater than the incremental attenuation caused by each additional wall [17].

Multi-Wall-and-Floor model takes into account the decreasing penetration loss of walls and floors of the same category as the number of traversed walls/floors increase. The walls and floors that have to be considered are determined by the Obstructed Line-Of- Sight (OLOS) path. The equation for the model is given by [17],

$$L = L_0 + N \log d + \sum_{i=1}^{I} \sum_{k=1}^{K_{wi}} L_{wik} + \sum_{j=1}^{J} \sum_{k=1}^{K_{fj}} L_{fjk}, \tag{2.9}$$

where I is number of wall types, J number of floor types, L_{wik} is attenuation due to wall type i and k-th traversed wall, L_{fjk} is attenuation due to floor type j and k-th traversed floor, K_{wi} is number of traversed walls of category i and K_{fj} number of traversed floors of category j.

Model coefficients at 5.8 GHz were provided in [17].

2.10. Winner II Model

WINNER II channel model was proposed for indoor, indoor to outdoor, outdoor to indoor, and outdoor scenarios. Firstly, the model is applied at 2 and 5 GHz, then

it is extended over frequency range 2-6 GHz. The general equation for the model is given in Equation 2.10 [18].

$$L = A \log d[\text{m}] + B + C \log \left(\frac{f_c[\text{GHz}]}{5} \right) + X + FL, \tag{2.10}$$

where A is path loss exponent, B is the intercept, C is path loss frequency dependence parameter and X is wall attenuation term for indoor scenario.

Model coefficients for frequency range 2 GHz-6 GHz were given in Table 2.10 [17].

Table 2.10. Model coefficients for WINNER II model.

Scenario	Coefficients	Standard Deviation
LOS	$A = 18.7, B = 46.8, C = 20$ $X = 0$	$\sigma = 3$
Corridor-to-Room NLOS (Light Walls)	$A = 36.8, B = 43.8, C = 20$ $X = (5n_w - 1)$	$\sigma = 3$
Corridor-to-Room NLOS (Heavy Walls)	$A = 36.8, B = 43.8, C = 20$ $X = (12n_w - 1)$	$\sigma = 4$
Room-to-Room NLOS (Light Walls)	$A = 20, B = 46.4, C = 20$ $X = 5n_w$	$\sigma = 6$
Room-to-Room NLOS (Heavy Walls)	$A = 20, B = 46.4, C = 20$ $X = 12n_w$	$\sigma = 8$
Floor Loss	$FL = 17 + 4(n_f - 1)$	-

2.11. Lecours Model

Lecours model calculates propagation loss as a free space loss and additional losses caused by effects of walls, floors, diffraction, reflection and furnitures. 729 measurements were conducted at 917 MHz in [19]. The modeling fits the data within ± 2

dB for 68% of the 729 measurements, the standard deviation between measurements and prediction are slightly less than 3 dB.

The general formula for the model is expressed as,

$$P_R = P_T + G_T + G_R + L_F + L_{OB} + G_{RM}, \tag{2.11}$$

where P_R is the received power, P_T is the transmitted power, G_T is the transmitter antenna gain, G_R is the receiver antenna gain, L_F is free space loss, L_{OB} is loss due to obstacles and G_{RM} is the gain due to reflections.

The model tries to estimate L_{OB} and G_{RM} values for variety of indoor propagation conditions. For wall losses, L_{OB} is given by [19],

$$L_{OB} = 3.7 - 1.5n - 10.7 \log d + \begin{cases} 0 & d' < 4m, \\ -7.8 + 15.3 \log d' & d' \geq 4m, \end{cases} \tag{2.12}$$

where n is the number of walls and d' is the distance between transmitter and the first wall.

When d' distance becomes larger than 4 m, there is a change of slope. Authors of [19] also provide a way to differentiate between ordinary walls and corners, thin walls and thick walls. For corners, $n = 1$, for thin walls, $n = 1/2$ and for thick walls, $n = 2$ values are suggested.

Floor loss is given by [19],

$$L_{OB_{final}} = L_{OB_{initial}} - 27.5 - 41.7 \log p, \tag{2.13}$$

where p is the number of floors.

Reflection plays a significant role for corridors without transversal doors. Reflec-

tion in these scenarios generates higher received power than predicted by free space loss. In order to model reflection gain, the model offers the following modification [19],

$$G_{RM} = 0.2 + 1.8 \log d. \tag{2.14}$$

For reflection effect in corridors with transversal doors, the following equation is suggested [19],

$$G_{RM} = b_k + m \log d, \tag{2.15}$$

where $m = -0.0067k^2 + 2.35$, $b_k = P_k - m \log k$, k is distance between transmitter and the last obstructing door and P_k is signal level estimated at k m.

Two diffraction scenarios are taken into account in [19]. These diffraction conditions are shown in Figure 2.3.

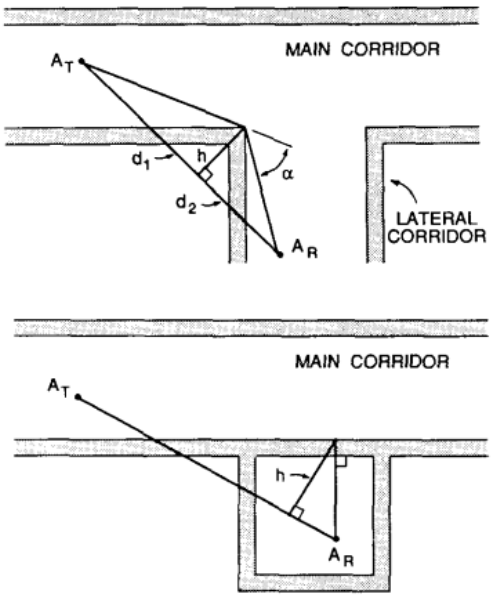

Figure 2.3. Diffraction cases for Lecours model.

Equation 2.16 is used for the first scenario in which lateral corridor opens on main corridor. Equation 2.17 is used for the second scenario in which room is adjacent to

corridor [19].

$$L_{OB} = -5.6 - 12 \log h + 1, \tag{2.16}$$

$$L_{OB} = -7.6 - 11.5 \log h + 1, \tag{2.17}$$

2.12. Reduced Complexity UTD Indoor Model

Because of huge complexity of physical models, it is very hard to implement purely physical models to indoor environment without excessive work. An approach proposed in [20] incorporates much of the propagation phenomena suggested by electromagnetic theory, such as UTD, but still retains the straightforwardness of the empirical approach. Potential advantage of this is that the empirical factors required in the model can be related closely to the theoretical derivations so that fitting or optimization of the model to propagation data will not necessarily be required. Another advantage of this is that computation time can be kept to a minimum so that predictions can be performed interactively on a computer without a significant reduction in prediction accuracy.

Reduced Complexity UTD Indoor Model takes the following factors into account:

- Dual-Slope path loss with a break-point distance.
- Wall penetration losses.
- Floor penetration losses.
- Angle between incident wave and obstructing wall.
- Angle between incident wave and obstructing floor.
- One-level of diffraction from corners.

The resulting model is given by [20],

$$\begin{aligned} L(r) =& 10 \log \left(\frac{r}{r_0} \right)^{n_1} u(r_b - r) \\ &+ 10 \left[\log \left(\frac{r_b}{r_0} \right)^{n_1} + \log \left(\frac{r}{r_b} \right)^{n_2} \right] u(r - r_b) \\ &+ \sum_{i=1}^{W} \frac{n_{wi} L_{wi}}{\cos \theta_i} + \sum_{i=1}^{W} \frac{n_{fi} L_{fi}}{\cos \theta_j}, \end{aligned} \tag{2.18}$$

where r_b is break-point distance, L_{wi} is wall loss, L_{fi} is floor loss, n_{wi} is number of walls, n_{fi} is number of floors and $u(.)$ is unit step function.

To keep the diffraction model simple, the authors in [20] utilise only one level of diffraction from corners, including door and window frames in the building. To perform this, the field is calculated at each corner using Equation 2.18 and the resulting diffracted field is determined using a diffraction coefficient. Thus, the total field at the receiver is computed as the summation of the field from the transmitter and all the corners.

Diffraction coefficients for perfect electrical conductors in [21] are used in the model and are denoted as $D(r, \phi, r', \phi')$, where (r, ϕ) are the coordinates of the corner relative to the transmitter and (r', ϕ') are the coordinates of the receiver relative to the corner. The final equation is then given by,

$$L_T = -10 \log \left[\sum_{m=1}^{M} (l_L(r_m) l_L(r_{m'}) \times |D(r_m, \phi_m, r'_m, \phi'_m)|^2) + l_L(r) \right], \tag{2.19}$$

where M is the number of corners in the building database and $l_L(.)$ is a dimensionless quantity given by,

$$l_L(.) = 10^{-L(.)/10}. \tag{2.20}$$

Measurements were conducted at 900 MHz in [20] to determine model coefficients.

These parameters are given in Table 2.11.

Table 2.11. Model coefficients for Reduced Complexity UTD Indoor model.

n_1	n_2	r_b[m]	L_w[dB] (Concrete)	$L_w[dB]$ (Plasterboard)
1	2.5	10	10	5

Authors of [20] conducted variety of measurements and tested both Motley-Keenan model and their proposed model. Predicted path loss vs measured path loss graphs for Motley-Keenan model and UTD indoor model is shown in Figures 2.4 and 2.5 [20]. UTD indoor model performs better than Motley-Keenan model in low-loss

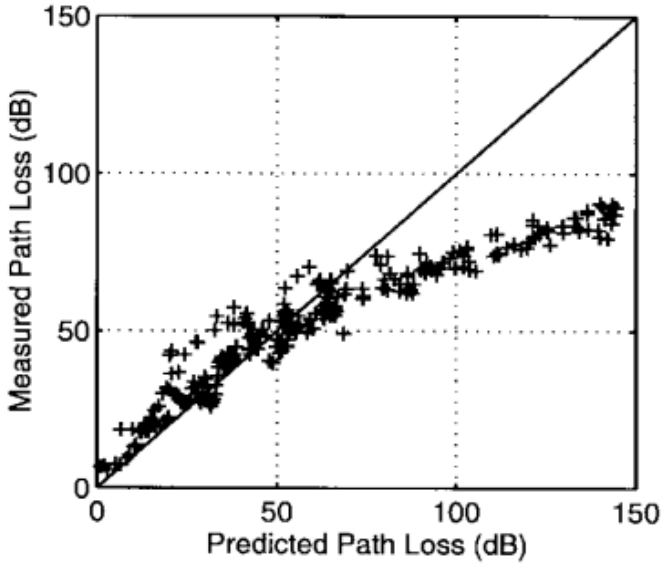

Figure 2.4. Scatter plot of predicted versus measured path loss for Motley-Keenan model.

regions but the most striking difference is in the high loss regions where Motley-Keenan model overestimates the actual path loss by up to 40 dB as evidenced by the downward curving scatter plot. This overestimation corresponds to measurement samples from the upper right region of the floor plan where the actual path loss is largest. The reason Motley-Keenan model performs poorly in this region is that the direct path becomes blocked by the large number of walls between the transmitter and receiver, thus making Motley-Keenan model predict a large propagation loss. UTD indoor model, however,

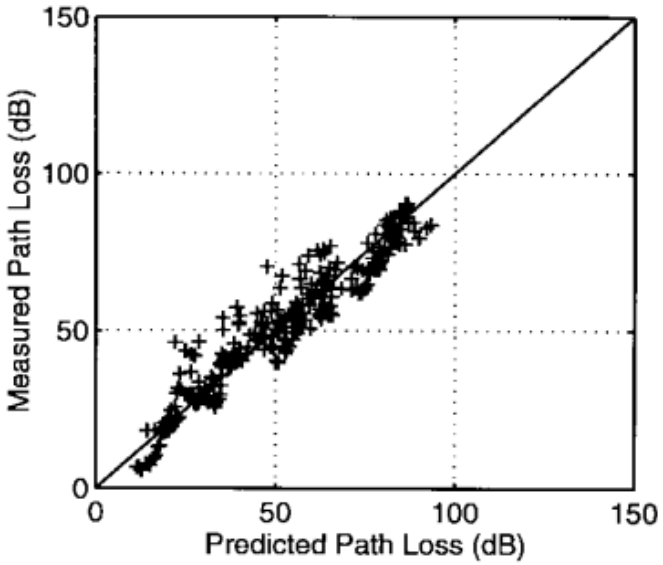

Figure 2.5. Scatter plot of predicted versus measured path loss UTD indoor model.

finds that the actual path loss is less because there is a diffracted path that exists from the door frames along the lower corridor through only two rooms to the upper corridor. Statistics of the comparisons between the two models are shown in Table 2.12 [20].

Table 2.12. Statistics of the comparisons between Motley-Keenan model and UTD Indoor model.

Model	Mean Error[dB]	σ[dB]	% error$<\pm$ 5 dB	% error$<\pm$ 10 dB
UTD Indoor Model	-0.3	6.7	54.0	86.8
Motley-Keenan Model	14.8	20.8	33.8	56.8

2.13. Through-Wall Physical Model

Room to room propagation model utilizing theoretical calculation of wall losses was proposed in [22]. This model improves Equation 1.3 by adding a through-wall loss factor to it. Through-Wall Physical Model uses single-ray launching techniques and assumes that in walls with relatively small conductivity, the transmitted wave is practically uniform at typical mobile communications frequencies.

The wall is represented as an infinite homogeneous flat plate with two electric parameters, relative permittivity $\epsilon_r = \epsilon/\epsilon_0$ and conductivity σ , and thickness d. Propagation mechanism used by the model is shown in Figure 2.6. Propagation constant of

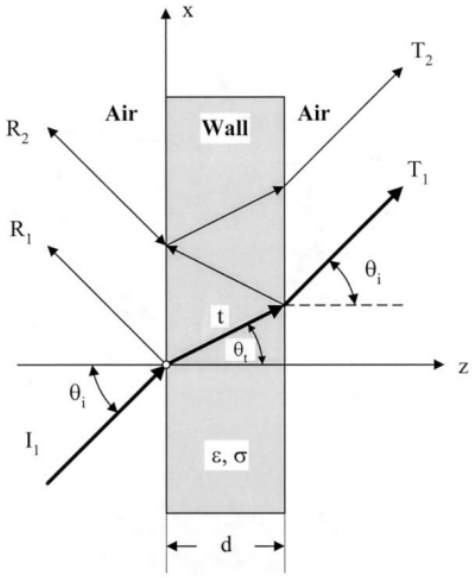

Figure 2.6. Through-Wall Propagation.

the wall $\gamma = \alpha + j\beta$ is calculated using the following formula [22],

$$\begin{pmatrix}\alpha\\ \beta\end{pmatrix} = w\sqrt{\mu_0\epsilon_0\epsilon_r}\sqrt{\frac{1}{2}\left[\begin{pmatrix}-1\\ +1\end{pmatrix} + \sqrt{1+\left(\frac{\sigma}{w\epsilon_0\epsilon_r}\right)^2}\right]}. \tag{2.21}$$

The amplitude transmission coefficient (T) for a propagation depicted in Figure 2.6 is given by [22],

$$T = T_{12}A, \tag{2.22}$$

where $T_{12} = |T_1T_2|$. T_1 is the Fresnel transmission coefficient at the plane $z = 0$, equal to $T_1^{\perp}$ or $T_1^{\parallel}$, depending on the polarization. T_2 is the Fresnel transmission coefficient at the plane $z = d$, equal to $T_2^{\perp}$ or $T_2^{\parallel}$. A is amplitude attenuation factor due only to the wall absorption losses along the inner transmission path and it is given as an

exponential attenuation function,

$$A = e^{-\alpha t}. \tag{2.23}$$

Conductivity and relative permittivity of different wall types are widely available in the literature. Using these values, it is easy to calculate attenuation factor using the Equation 2.21. With attenuation factor known, Equation 2.23 is used to estimate wall absorption loss.

The coefficients T_1 and T_2 account for the attenuation due to the mismatch between air and wall media only or, equivalently, the attenuation, if the same wall is thought to be a lossless dielectric plate ($\sigma = 0$). For a lossless homogenous wall embedded in air, it is easy to derive the transmission coefficient T_{12} for both polarizations, as a function of ϵ_r and θ_i [22],

$$T_{12}^{\perp} = \left| \frac{4\cos\theta_i \sqrt{\epsilon_r - \sin^2\theta_i}}{(\cos\theta_i + \sqrt{\epsilon_r - \sin^2\theta_i})^2} \right|, \tag{2.24}$$

$$T_{12}^{\parallel} = \left| \frac{4\epsilon_r \cos\theta_i \sqrt{\epsilon_r - \sin^2\theta_i}}{(\epsilon_r \cos\theta_i + \sqrt{\epsilon_r - \sin^2\theta_i})^2} \right|. \tag{2.25}$$

Dependence of the amplitude transmission coefficient T on the relative permittivity and conductivity are provided in [22]. These are shown in Figures 2.7 and 2.8. Figure 2.7 tells us that for $\epsilon_r = 3$ to 9 the transmission coefficient varies by less than 3 dB. It is seen in Figure 2.8 that transmission coefficient changes by around 16 dB for the typical range of values for $\sigma = 0.01$ S/m to 0.1 S/m [22].

Equations 2.24 and 2.25 show that transmission coefficient is tied to angle of incidence as well. Authors of [22] provide graphs for variation of received power by angle of incidence for brick and concrete walls. The graph for concrete wall is shown

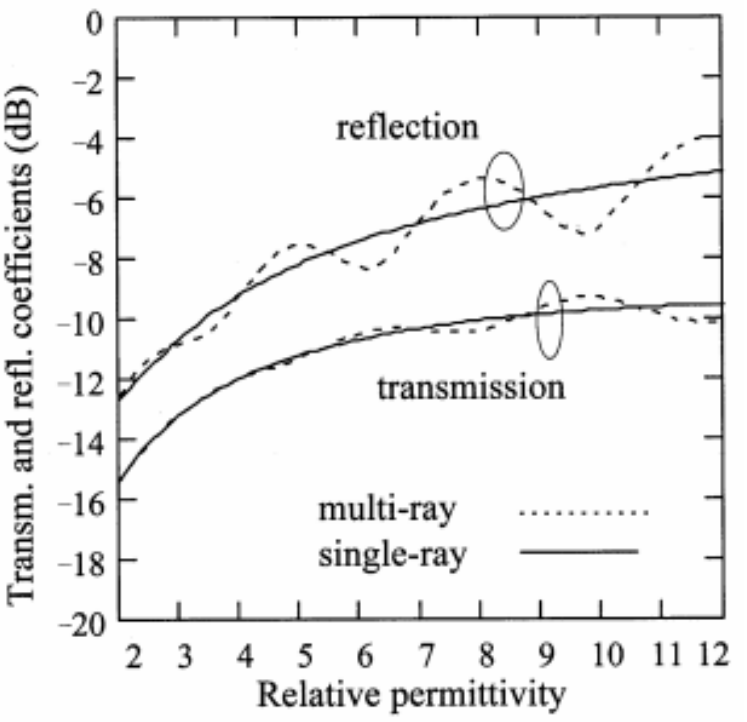

Figure 2.7. Transmission and reflection coefficient versus permittivity.

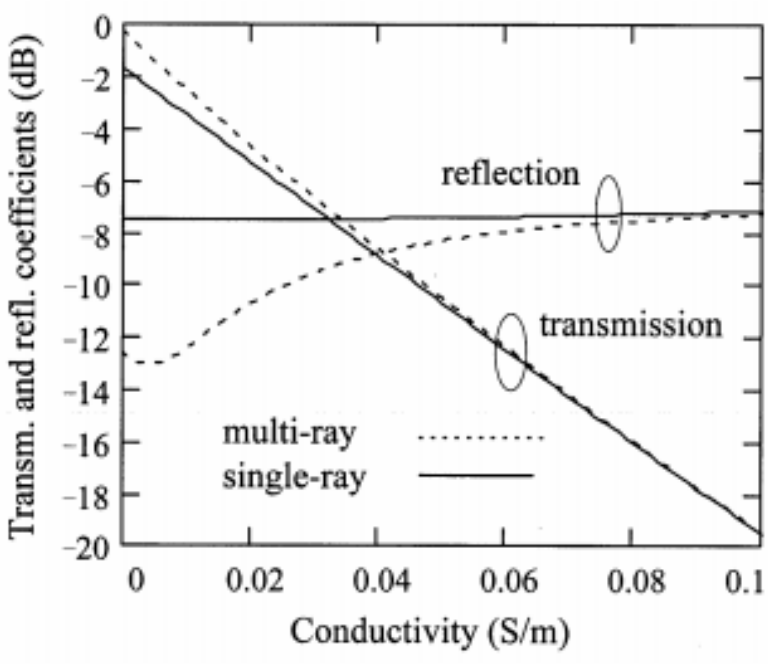

Figure 2.8. Transmission and reflection coefficient versus conductivity.

in Figure 2.9. The results in the model could be summed such that propagation loss

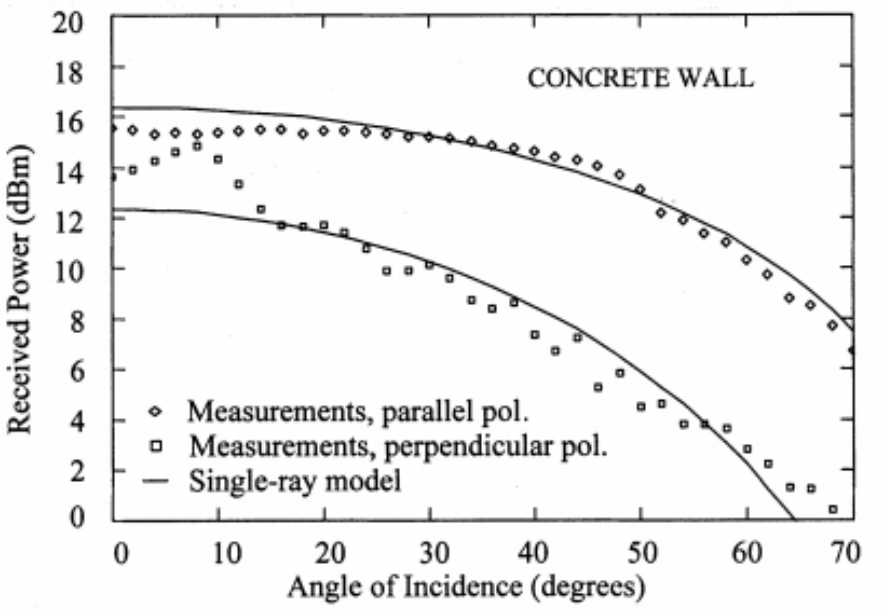

Figure 2.9. Received power versus angle of incidence for concrete wall.

through a different medium depends on conductivity and thickness of the obstructing material and angle of incidence. Authors of [22] then present a model which modifies the Friis equation by adding through-wall power loss expressed by the power transmission coefficient T^2. The equation obtained is shown as,

$$\begin{aligned} P_r(\text{dBm}) = P_t(\text{dBm}) + G_t(\text{dB}) + G_r(\text{dB}) + 20\log T \\ -20\log f(\text{MHz}) - 20\log r(\text{m}) + 27.6, \end{aligned} \tag{2.26}$$

where P_r and P_t are the powers at the receiver and transmitter antenna output and input; G_r and G_t are the receiver or transmitter antenna gain, respectively; and r is the distance between receiving and transmitting antenna, corresponding to line-of-sight distance in free space.

Experimental results of this model for brick and steel-reinforced concrete walls are included in [22]. Authors of [22] use the model to determine the ϵ_r and σ values of a wall from measured input power values.

3. MEASUREMENTS AND MODEL IMPLEMENTATION

In the first section of this chapter, procedure and details of the measurements are explained. In the second section, measurement results for specific receiver-transmitter configurations are included and the models described in Chapter 2 are implemented to estimate receiver power for the same measurement configurations. In the last section of the chapter, strengths and weaknesses of models are evaluated.

3.1. Measurement Procedure

Two floors of NETAS Office building; 3rd and 4th floors are used for measurements. All the same floor measurements are conducted in the 3rd floor while 4th floor is used for multi-floor propagation measurements. Photos of the office environment are given in Figure 3.1 and Figure 3.2.

Figure 3.1. First view of NETAS Office.

Figure 3.2. Second view of NETAS Office.

A signal generator from 10 MHz to 20 GHz is used to generate electromagnetic signals. For an antenna, omnidirectional dual-band GSM mag-mount antenna from Pasternack is used at both transmitter and receiver sides. Antenna attached to signal generator is assumed to be a picocell base station while antenna attached to spectrum analyzer is assumed to be a cellphone. Picture of the antennas used is shown in Figure 3.3. Specifications of the antennas are listed in Table 3.1.

Figure 3.3. Omnidirectional GSM antenna used in the measurements.

Table 3.1. Specifications of the antenna used in the measurements.

Parameter	Value
Band1 Frequency	890-960 MHz
Band2 Frequency	1710-1880 MHz
Impedance	50 Ohms
Gain	3 dBi

Before beginning the indoor office measurements, free-space calibration is conducted in the open terrain near the office building. Free-space calibration is needed to determine exact antenna gains at frequencies of interest and thus find only path loss component of any measurement. For this purpose, three measurements at 10 m, 20 m and 30 m are taken. Free-space loss predicted by Friis equation is then compared to actual measurement results and the difference is taken as antenna gains minus attenuation caused by cables. Cable loss of spectrum analyzer is measured by directly

connecting analyzer to signal generator and found as 1.2 dB at 900 MHz and 2 dB at 1800 MHz. Antenna cables are specified as 5 meters of RG174/U type coaxial cables. Attenuation of 5 m of this type of cable is found in the internet as 4.5 dB at 900 MHz and 7 dB at 1800 MHz. Substracting these cable attenuations from free-space loss, antenna gains for 900 MHz and 1800 MHz are found.

70 measurements are taken with different transmitter-receiver locations for model testing. +15 dBm input power is applied for both 900 MHz and 1800 MHz measurements. Received signal levels as low as −110 dBm are measured. Measurement results are shown in Section 3.2. Experimental setup with signal generator, spectrum analyzer, transmit-receive antennas and a laser distance meter are shown in Figure 3.4.

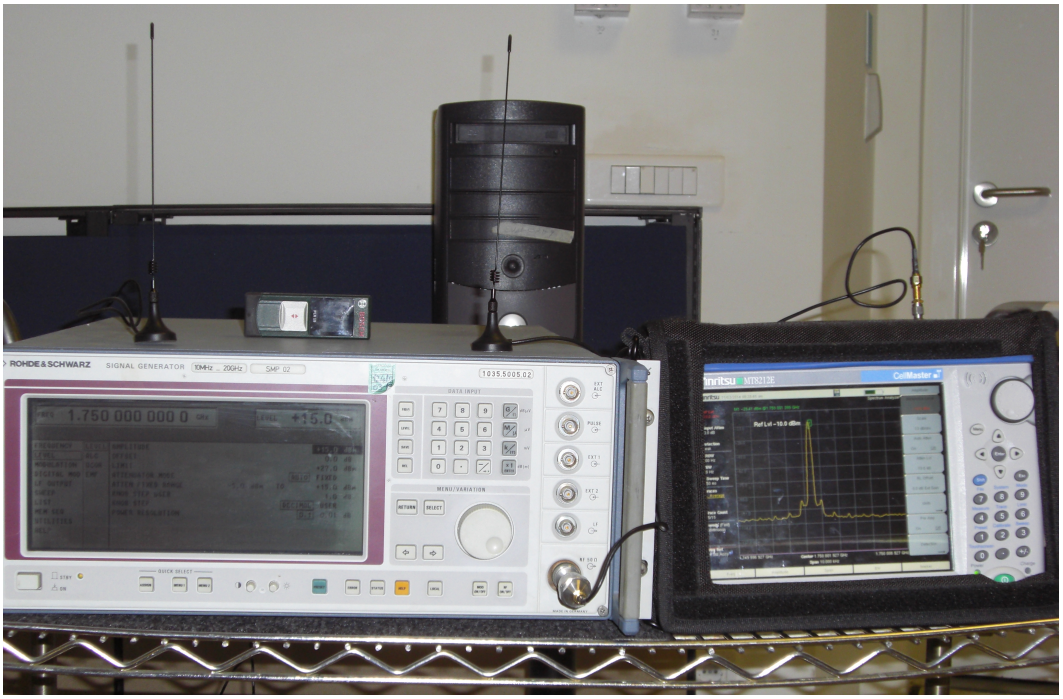

Figure 3.4. Experimental setup.

Transmitter is placed in several different locations and for each transmitter location, measurements are taken while receiver position is moved to different positions. This process is repeated many times and a total of 70 measurements are taken. Measurement positions are shown in Figure 3.5 and Figure 3.6. Location of desired measurement point is selected on the map and transmitter and receiver is placed in the exact place with lasermeter being used to achieve accurate placement.

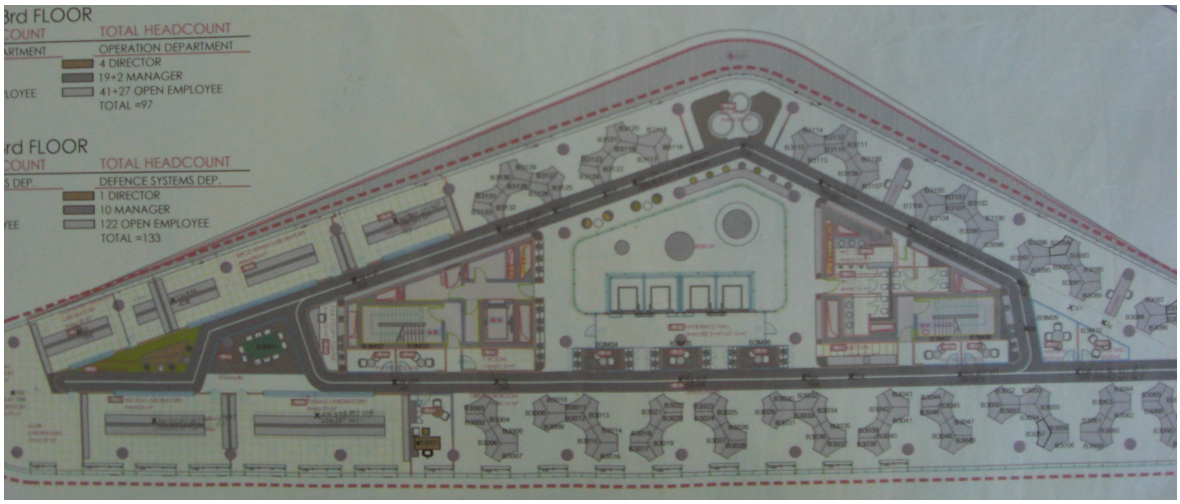

Figure 3.5. Measurement Positions I.

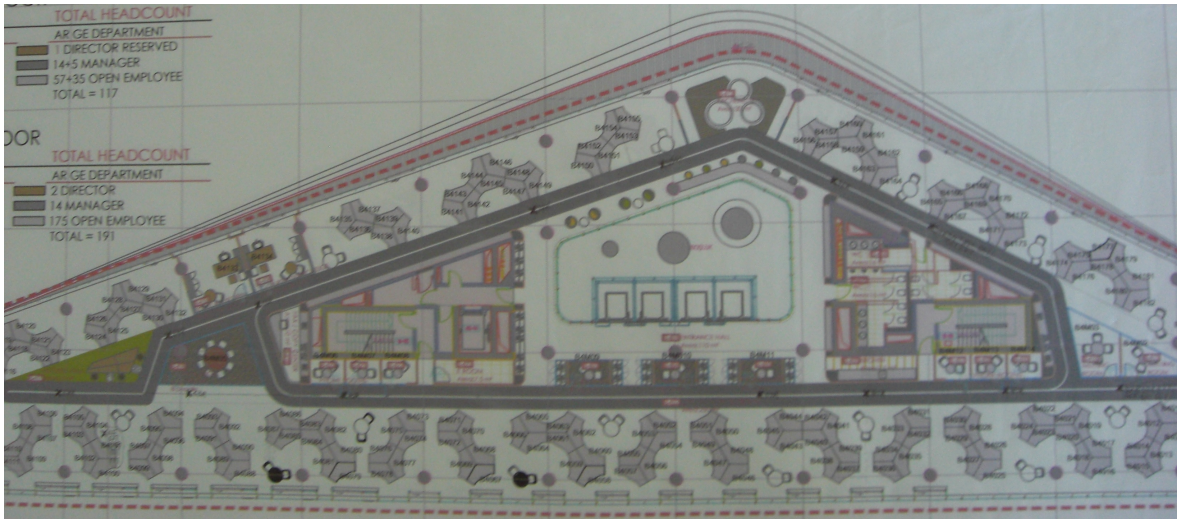

Figure 3.6. Measurement Positions II.

3.2. Model Implementation

Respective formula of each model is realized in MATLAB with model parameters given as inputs. Each measurement scenario which is marked on the floor maps is then analyzed and necessary model inputs are determined. These inputs include distance, number of walls, thickness of walls, types of walls, number of floors, number of corners, and etc. Propagation loss of each model is then compared to actual propagation loss results in graphs. The last 17 measurements in the graphs are multi-floor measurements. Mean absolute error of all models are calculated for single-floor, multi-floor, line-of-sight, light obstruction by plaster walls and heavy obstruction by concrete walls

scenarios seperately. The reason for this is to evaluate model's performance for different scenarios.

3.2.1. Through-Wall Physical Model

Through-Wall Physical model presented wall loss as a function of permittivity, conductivity, thickness and angle of incidence. Effect of permittivity is shown to be a minor one in Section 2.13. Through-Wall physical model is used to find the attenuation levels of plaster walls, concrete walls and glass partitions in NETAS office.

In order to determine approximate attenuation factors for internal office walls, several test measurements are conducted. An empty laboratory in the second floor of NETAS office is used as a test environment. Transmitter and receiver are placed on two sides of obstructing walls to measure wall attenuation factors. Equation 2.26 is used to find $20 \log T$ factor which corresponds to wall attenuation in dB. Measured values of transmission coefficients and attenuation losses in dB for different obstructions are shown in Tables 3.2 and 3.3.

Table 3.2. Transmission coefficients for internal walls in NETAS office.

Wall Type	Thickness[cm]	900 MHz	1800 MHz
Glass	1	0.8	0.8
Plaster Wall	12	0.75	0.67
Concrete Wall	15	0.4	0.35

Table 3.3. Wall losses in dB for for internal walls in NETAS office.

Wall Type	Thickness[cm]	900 MHz	1800 MHz
Glass	1	2	2
Plaster Wall	12	2.5	3.5
Concrete Wall	15	8	9

Then measured values of transmission coefficents and attenuation values are com-

pared to the values found in the literature. *NIST Construction Automation Program Report* in [23] provides transmission coefficients for almost all construction materials while [24] gives attenuation values in dB for many types of walls.

For glass, G50L glass sample with thickness of 13 mm in [23] seems to to have similar results with glass partitions in our office. The transmission coefficient of G50L glass sample versus frequency is shown in Figure 3.7.

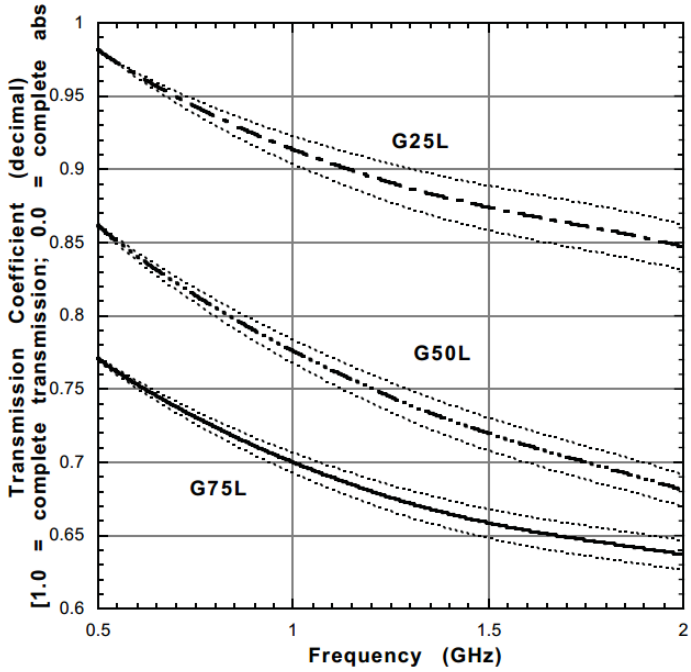

Figure 3.7. Transmission coefficent values for glass sample in NIST Report .

Transmission coefficent values of 0.78 and 0.74 are seen for 900 MHz and 1800 MHz respectively. These are very close to our measured value of 0.8 for both frequencies.

For concrete wall, C74L concrete sample with 102 mm is the best approximation. However, even though this sample is 50 mm thinner than our measurement sample, its results still overestimate concrete attenuation. The transmission coefficient of C74L concrete sample versus frequency is shown in Figure 3.8.

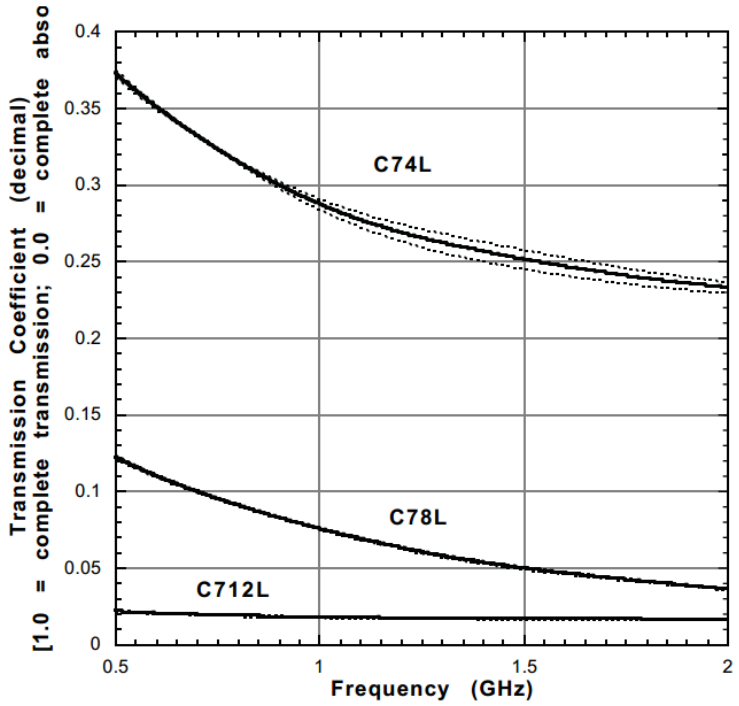

Figure 3.8. Transmission coefficent values for concrete sample in NIST Report .

NIST report measured transmission coefficient of 0.29 and 0.26 for concrete sample while our measured value is 0.4 and 0.35 for both 900 MHz and 1800 MHz respectively. Interpretation of this discrepancy should be the differences between concrete walls. For example, amount of metal in concrete walls greatly changes the conductivity and this in turn changes transmission coefficient as shown in Figure 2.8.

For plaster walls, NIST report provides results of only 6 mm, 13 mm and 16 mm drywalls. Our measurement wall is of 12 cm thick. Because of this, reference value in NIST report is not useful for comparison. Next, reference wall attenuation values for concrete and plaster walls in [24] are analyzed. This work shares some reference loss values that are very close to our measured values. These are shown in Table 3.4 [24].

Table 3.4. Reference wall losses for concrete and plaster walls.

Wall Type	Thickness[cm]	900 MHz	1800 MHz
Plaster Wall	20	4	6
Concrete Wall	20	8	9

It is shown that wall attenuation values predicted by Through-Wall Physical Model are reasonable and compatible with some reference values in the literature.

3.2.2. Single-Slope Model

Single-Slope model provides variety of L_0 and N values for different cases. For my measurements, *OPEN* case is used when there is LOS propagation or when transmitter and receiver are seperated by weak obstructions like glass, office desks and etc. *DENSE* case is used for all NLOS propagation scenarios. For different floor measurements, obvious *TWO-FLOORS* choice is used at first but this resulted in huge differences between measurement and model results. The floors in NETAS Headquarters are seperated by around 1.5 m thick wall and it nearly acts like two regular floors of standard apartment building. This behaviour is observed for all of the models. In order to compensate extra floor loss of NETAS office, *MULTI-FLOOR* case is used for different floor measurements.

Comparison of actual measurement loss to propagation loss predicted for the model at 900 MHz is shown in Figure 3.9.

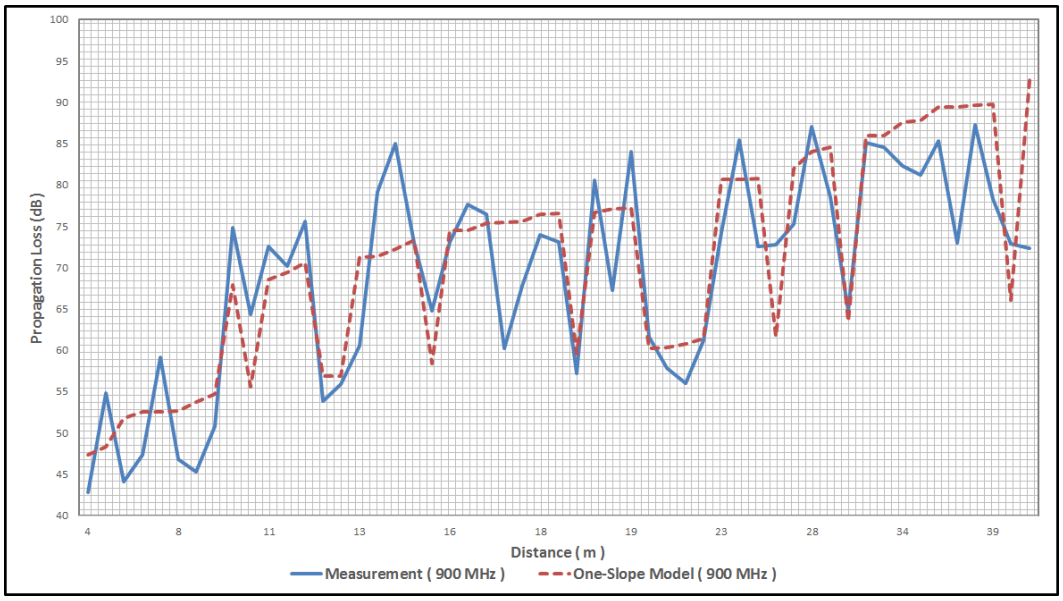

(a)

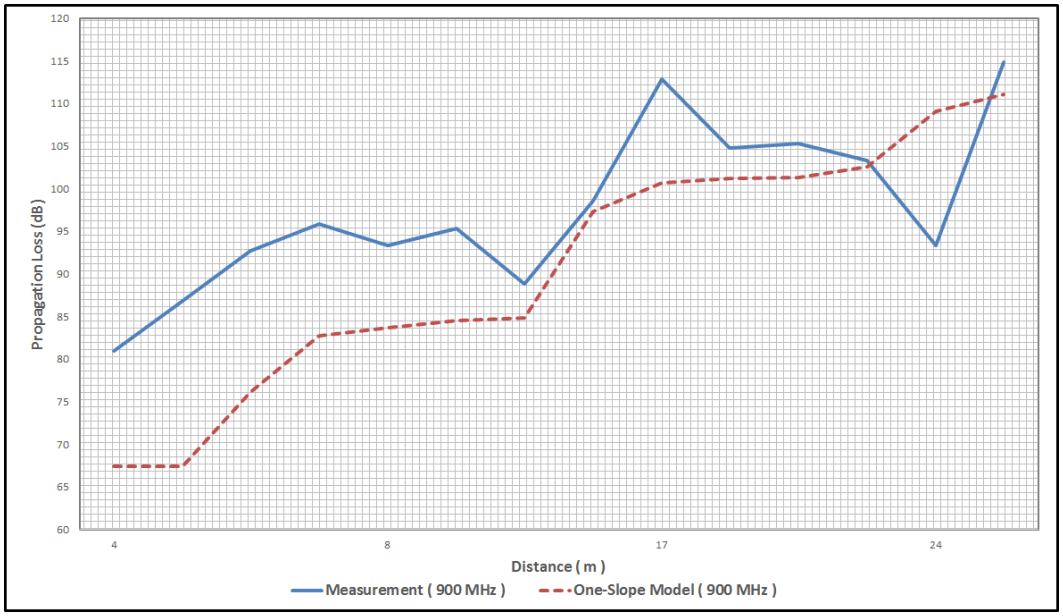

(b)

Figure 3.9. Comparison of Single-Slope model and measurement at 900 MHz, where (a) is for single-floor cases, (b) is for multi-floor cases.

Mean error values for different cases at 900 MHz are shown in Table 3.5.

Table 3.5. Mean error values for Single-Slope model at 900 MHz.

Case	Mean Error[dB]
Single-Floor	5.8
Multi-Floor	9.2
LOS	4.3
Light Obstruction	8.4
Heavy Obstruction	5.6

Comparison of actual measurement loss to propagation loss predicted for the model at 1800 MHz is shown in Figure 3.10.

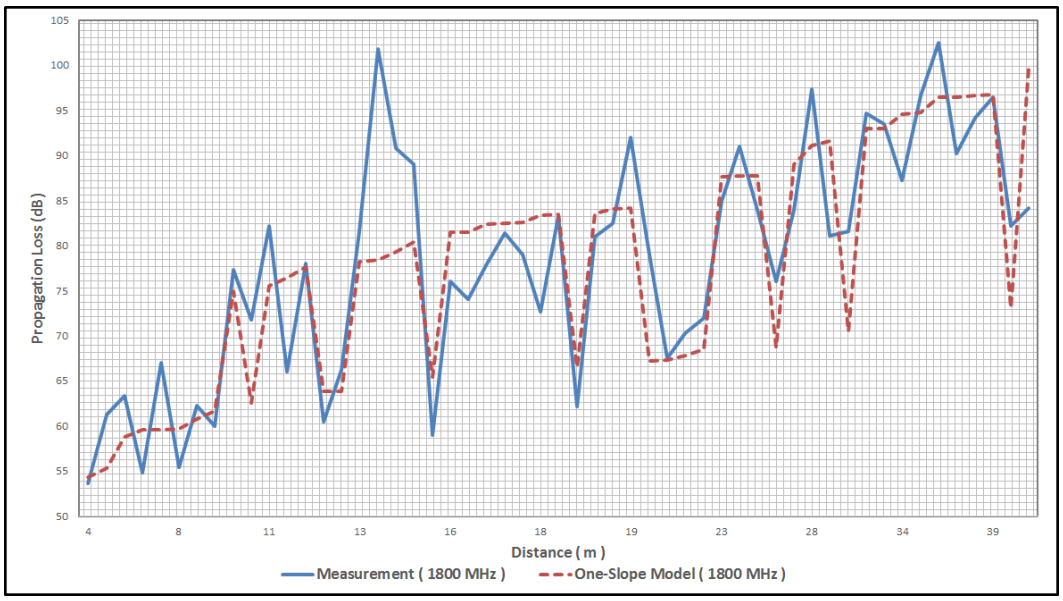

(a)

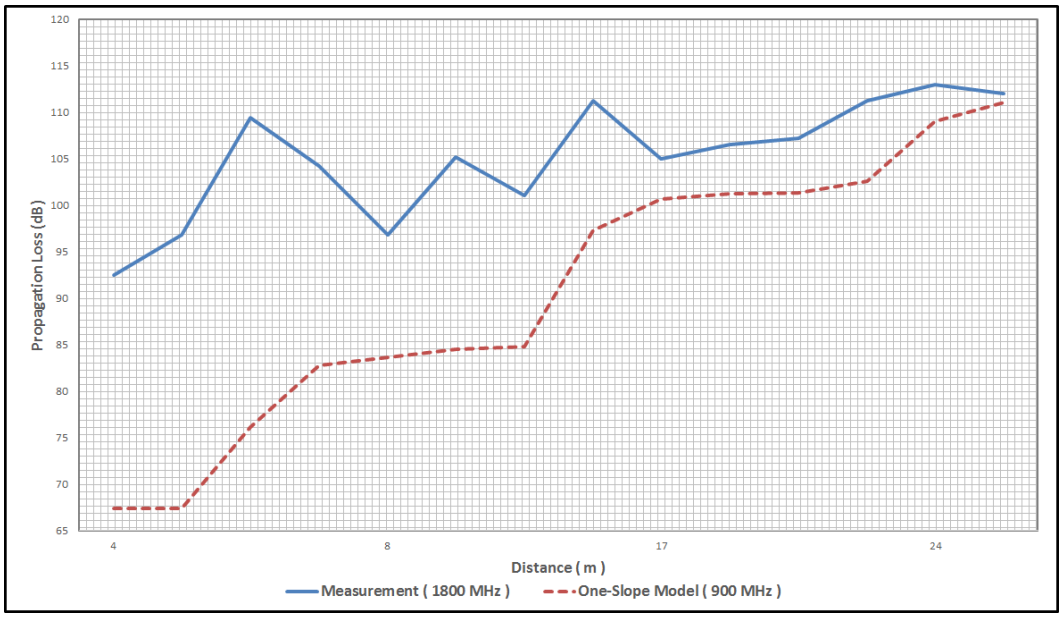

(b)

Figure 3.10. Comparison of Single-Slope model and measurement at 1800 MHz, where (a) is for single-floor cases, (b) is for multi-floor cases.

Mean error values for different cases at 1800 MHz are shown in Table 3.6.

Table 3.6. Mean error values for Single-Slope model at 1800 MHz.

Case	Mean Error[dB]
Single-Floor	5.4
Multi-Floor	8.9
LOS	3.1
Light Obstruction	6.5
Heavy Obstruction	6.1

Single-Slope model provides a good approximation for both 900 MHz and 1800 MHz with mean error of 5.4 dB. Although Single-Slope model does not account obstruction losses explicitly, *DENSE* case modification of L_0 and N values give good modeling of through-wall propagation. The only drawback of this approach is that in spite of a good mean error, overshoots and undershoots are common because of single-level evaluation of all obstructions. This can also be observed in high mean error difference between lightly-obstructed and heavily-obstructed cases. The model's single obstructed case formula fits better to concrete walls and this resulted in overshoots and higher mean error in lightly-obstructed cases. LOS propagation cases are also good with mean errors of 4.3 dB and 3.1 dB for 900 MHz and 1800 MHz respectively. It could be said that N value of 19 which the model suggested for *OPEN* cases is a good approximation for LOS propagation. *MULTI-FLOOR* case provided better results for different floor scenarios but still the results are worse than single-floor ones.

3.2.3. Dual-Slope Model

Dual-Slope model aims to achieve better transition from near-zone region with the addition of second-slope. N_2 value of 40 from Single-Slope model is used in Dual-Slope Model. N_1 of 20 is suggested in the literature, thus this value is used.

Comparison of actual measurement loss to propagation loss predicted for the

model at 900 MHz is shown in Figure 3.11.

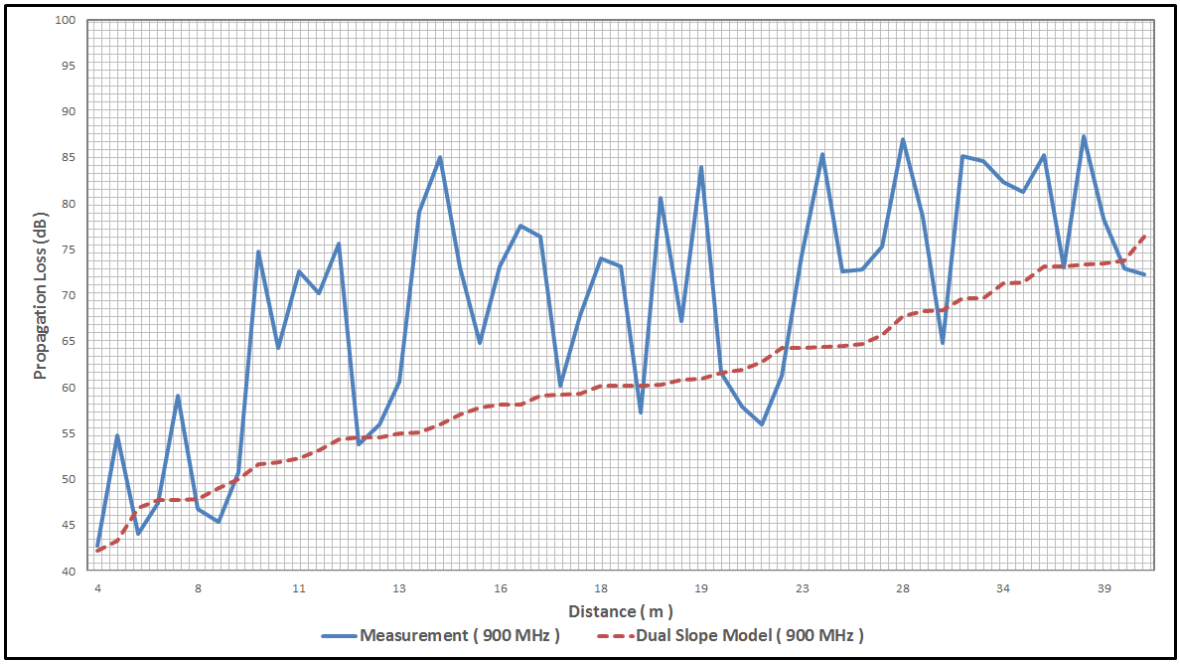

Figure 3.11. Comparison of Dual-Slope model and measurement at 900 MHz for single-floor cases.

Mean error values for different cases at 900 MHz are shown in Table 3.7.

Table 3.7. Mean error values for Dual-Slope model at 900 MHz.

Case	Mean Error[dB]
Single-Floor	10.2
Multi-Floor	44.3
LOS	2.7
Light Obstruction	6.3
Heavy Obstruction	14.5

Comparison of actual measurement loss to propagation loss predicted for the model at 1800 MHz is shown in Figure 3.12.

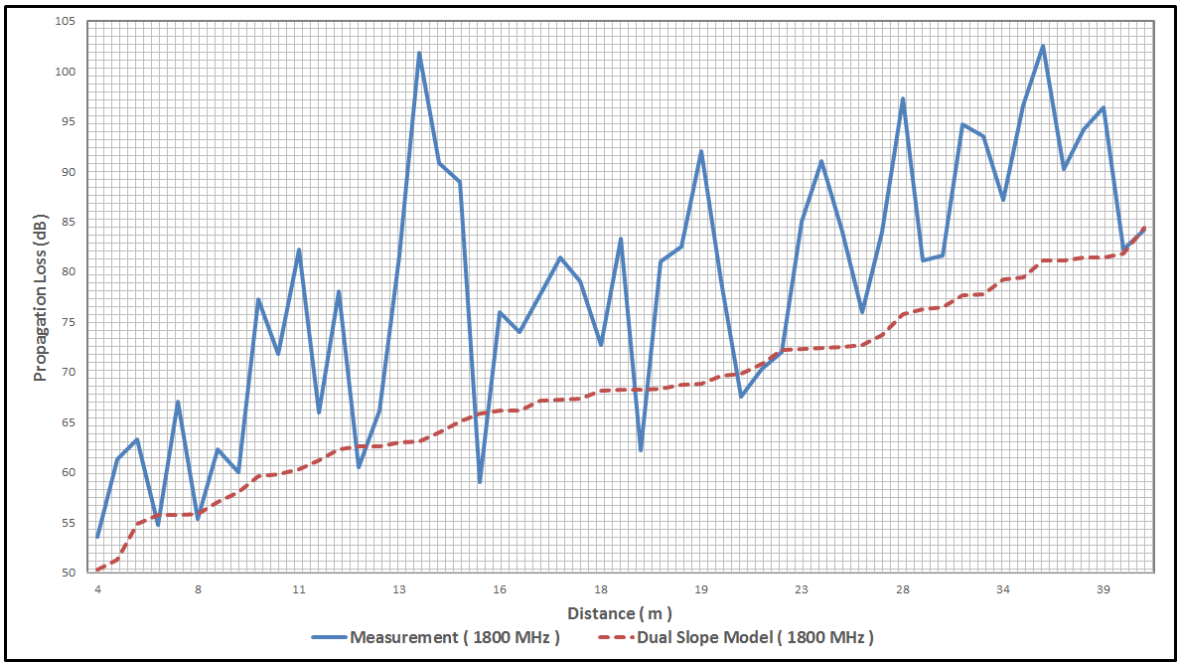

Figure 3.12. Comparison of Dual-Slope model and measurement at 1800 MHz for single-floor cases.

Mean error values for different cases at 1800 MHz are shown in Table 3.8.

Table 3.8. Mean error values for Dual-Slope model at 1800 MHz.

Case	Mean Error[dB]
Single-Floor	11.0
Multi-Floor	43.8
LOS	3.2
Light Obstruction	10.9
Heavy Obstruction	14.2

Dual-Slope model's LOS results are excellent because of addition of near-zone modeling of electromagnetic propagation. However, overall results are not good. This is somewhat expected as the model does not have different path loss exponent factors for propagation through obstructions. Because there is only one path loss exponent which is 40, accuracy decreases as the number of obstructions between transmitter and receiver increase. Path loss exponent of 40 becomes inadequate for concrete walls.

This issue is much more apparent for multi-floor scenarios. Dual-Slope model uses only distance as a factor. But in multi-floor scenarios, the distance is usually small but losses are very high because of floor loss. As a result, low distance coupled with high loss factor results in very inaccurate predictions for multi-floor cases.

3.2.4. ITU-R Model

ITU-R model modifies path loss exponent N to account for typical office environment losses. Floor loss is also added explicitly.

Comparison of actual measurement loss to propagation loss predicted for the model at 900 MHz is shown in Figure 3.13.

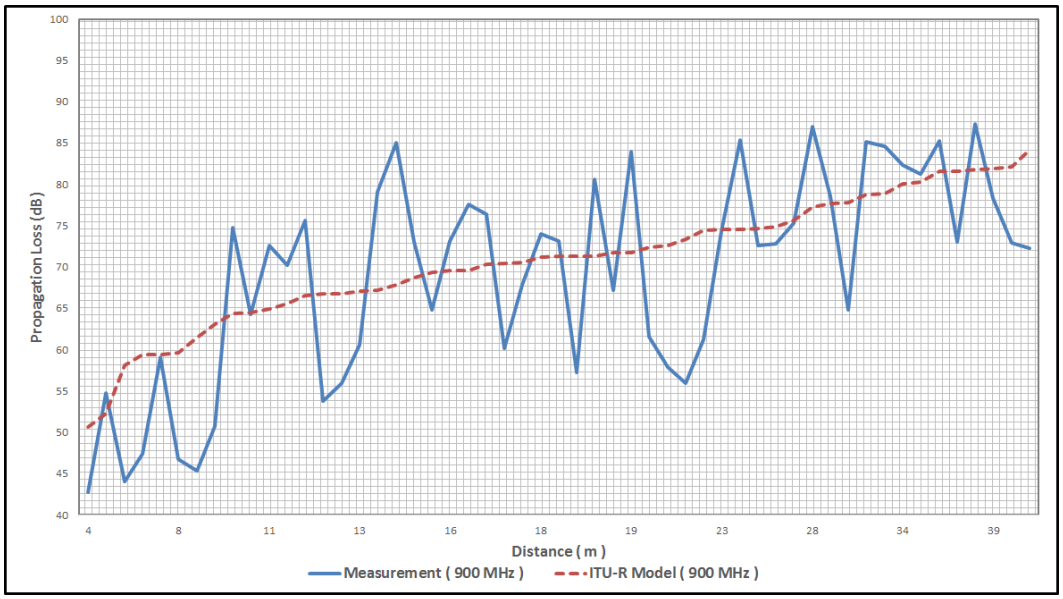

(a)

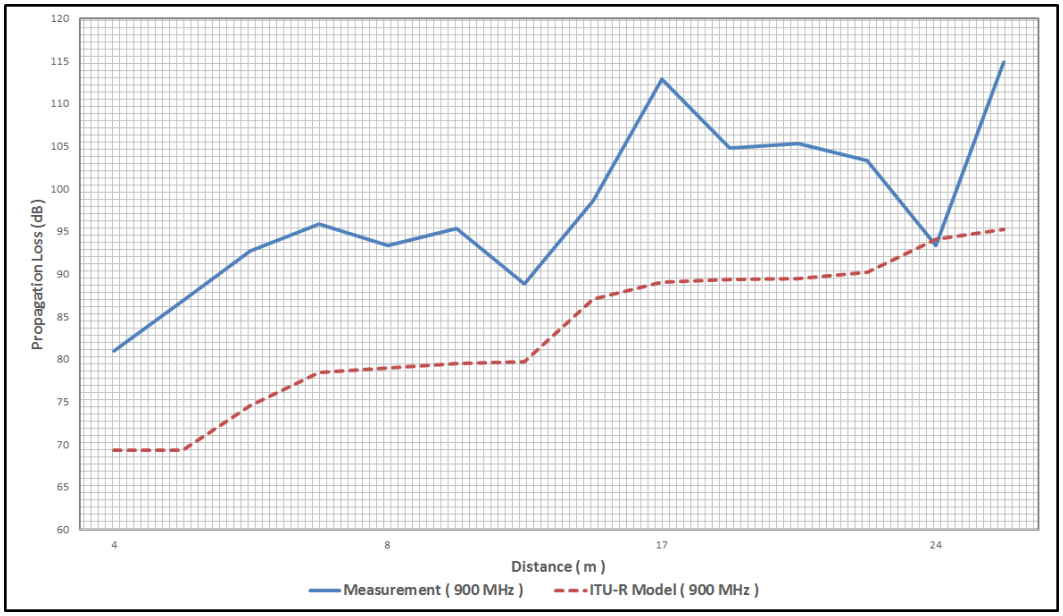

(b)

Figure 3.13. Comparison of ITU-R model and measurement at 900 MHz, where (a) is for single-floor cases, (b) is for multi-floor cases.

Mean error values for different cases at 900 MHz are shown in Table 3.9.

Table 3.9. Mean error values for ITU-R model at 900 MHz.

Case	Mean Error[dB]
Single-Floor	7.7
Multi-Floor	14.6
LOS	12.5
Light Obstruction	6.8
Heavy Obstruction	5.9

Comparison of actual measurement loss to propagation loss predicted for the model at 1800 MHz is shown in Figure 3.14.

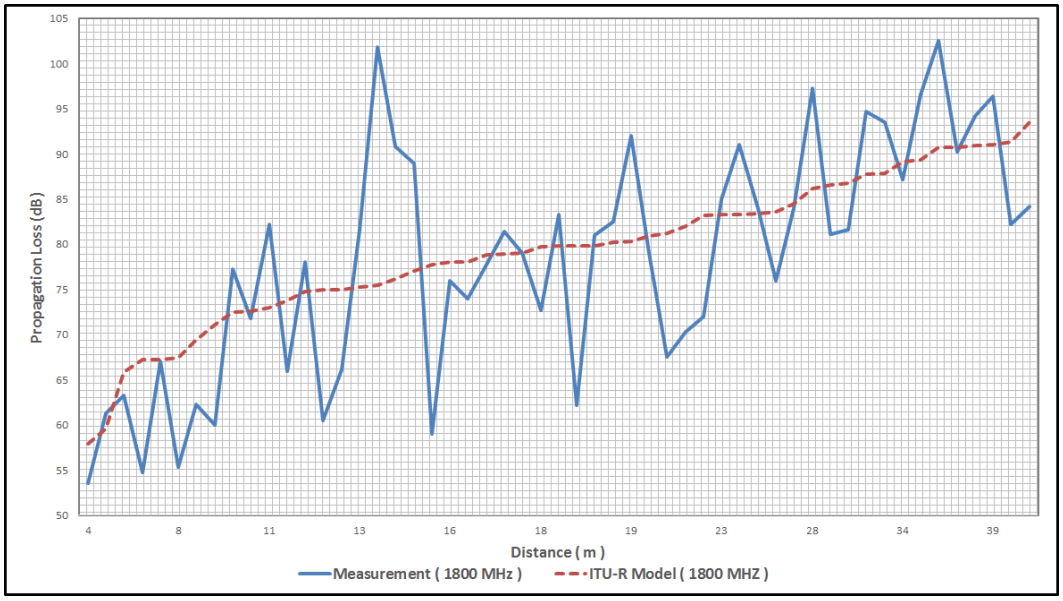

(a)

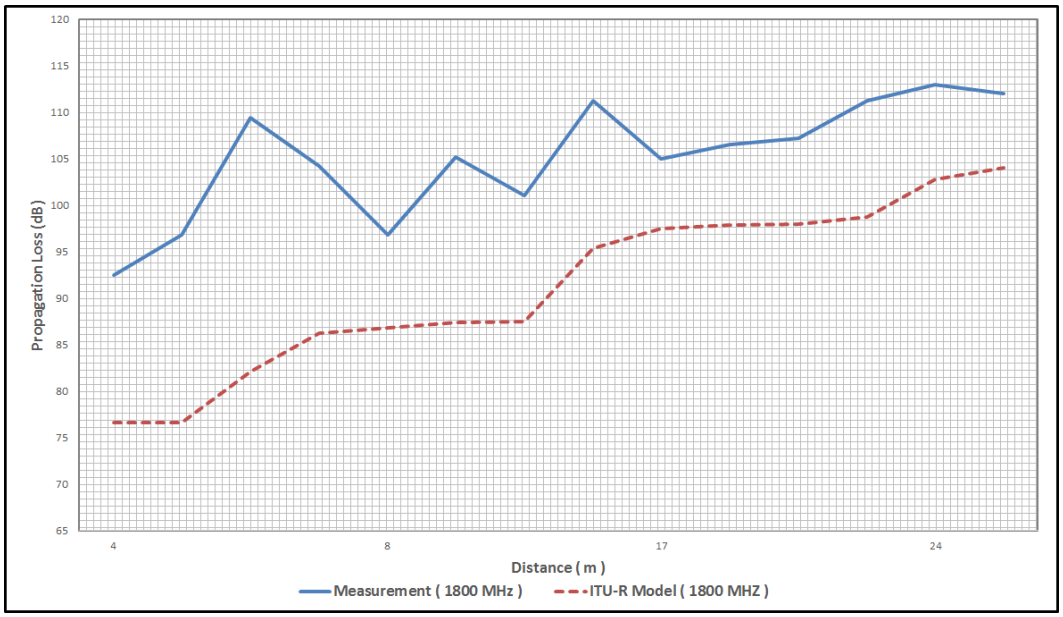

(b)

Figure 3.14. Comparison of ITU-R model and measurement at 900 MHz, where (a) is for single-floor cases, (b) is for multi-floor cases.

Mean error values for different cases at 1800 MHz are shown in Table 3.10.

Table 3.10. Mean error values for ITU-R model at 1800 MHz.

Case	Mean Error[dB]
Single-Floor	7.0
Multi-Floor	13.9
LOS	11.2
Light Obstruction	3.7
Heavy Obstruction	6.2

ITU-R model's overall mean error results are 7.7 dB and 7.0 dB for 900 MHz and 1800 MHz respectively. ITU-R model's modified path loss exponent yields acceptable predictions of light and heavy obstruction losses. However, this path loss exponent predicts much higher LOS losses than actual results because of the fact that while LOS propagation is mainly governed by path loss exponent of 20, ITU-R model uses path loss exponent of 30 and 33 for 900 MHz and 1800 MHz respectively. L_f value for two-floors are used as was the case with Single-Slope model. ITU-R model increases floor loss by 4 dB steps for each additional floors as shown in Table 2.4. So, there is only 4 dB difference between one floor and two floors. This underestimates the loss of floors in NETAS office. Due to this approach, mean error for multi-floor cases remained above 10 dB.

3.2.5. Motley-Keenan Model

Motley-Keenan model uses both modified path loss exponent and additional loss factors depending on the numbers of traversed walls and floors. L_f and L_1 values in Section 2.5 are used but floor attenuation factor a_f was too small for our office building. Floor attenuation factor of 40 dB is used for both 900 MHz and 1800 MHz based on our own measurements. There is no value specified for a_w in [14]. Wall attenuation factors for many materials are available in the literature. [24] provides shielding effectiveness values for many materials. In this model, 20 cm thick brick wall loss of 7 dB is

used for both 900 MHz and 1800 MHz. The reason for this choice is to approximate plasterboard, glass, concrete and high metallic furniture in our environment with an average value. If we take for example a reinforced concrete loss as a wall attenuation factor, that would overestimate losses in many scenarios at the expense of slightly better performance in few concrete-dominant cases.

Comparison of actual measurement loss to propagation loss predicted for the model at 900 MHz is shown in Figure 3.15.

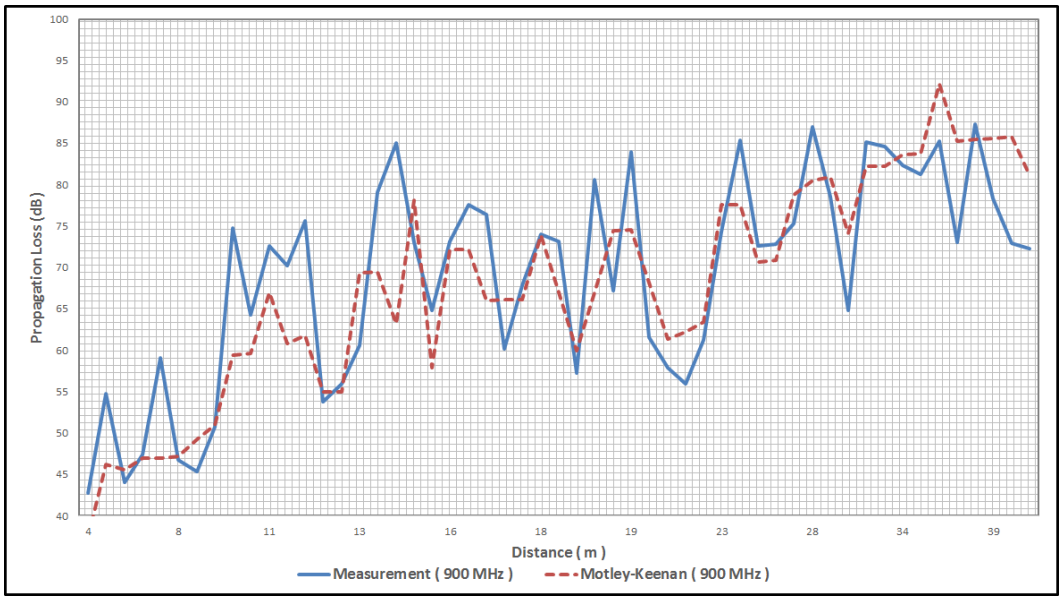

(a)

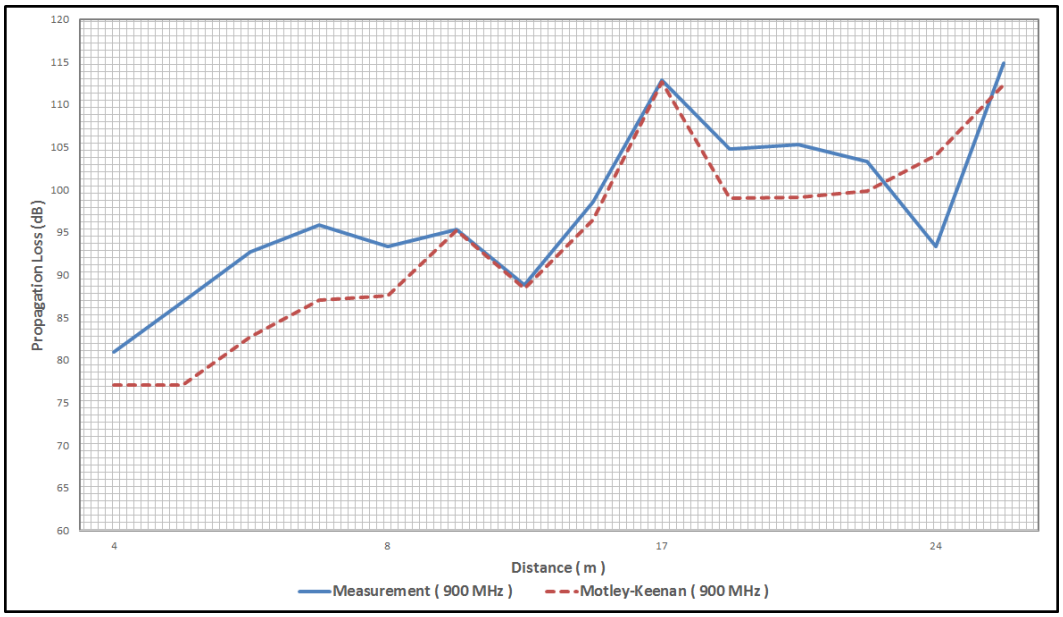

(b)

Figure 3.15. Comparison of Motley-Keenan model and measurement at 900 MHz, where (a) is for single-floor cases, (b) is for multi-floor cases.

Mean error values for different cases at 900 MHz are shown in Table 3.11.

Table 3.11. Mean error values for Motley-Keenan model at 900 MHz.

Case	Mean Error[dB]
Single-Floor	5.9
Multi-Floor	5
LOS	2.7
Light Obstruction	8.2
Heavy Obstruction	6.6

Comparison of actual measurement loss to propagation loss predicted for the model at 1800 MHz is shown in Figure 3.16.

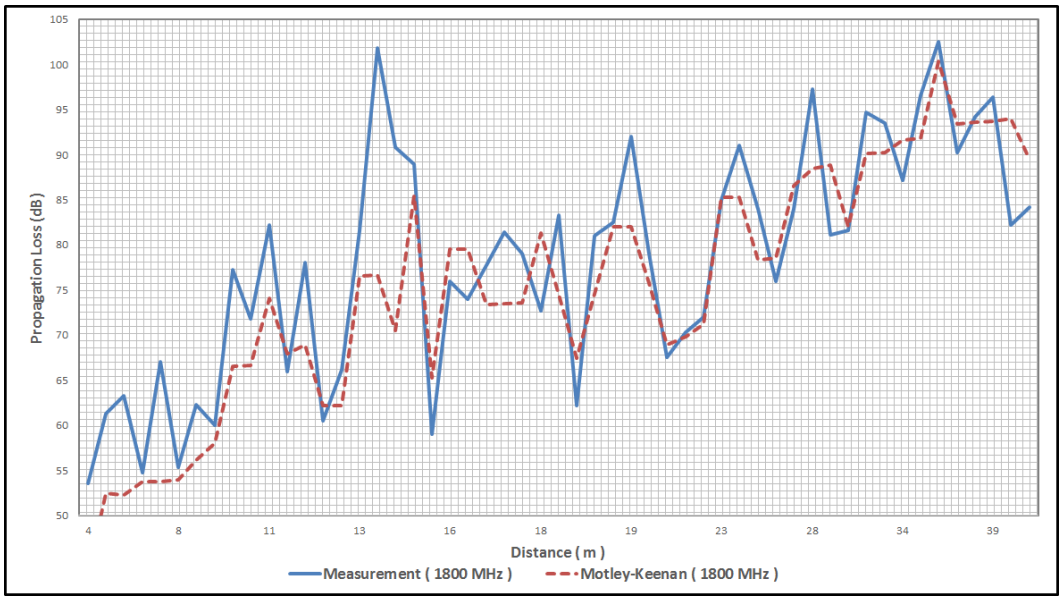

(a)

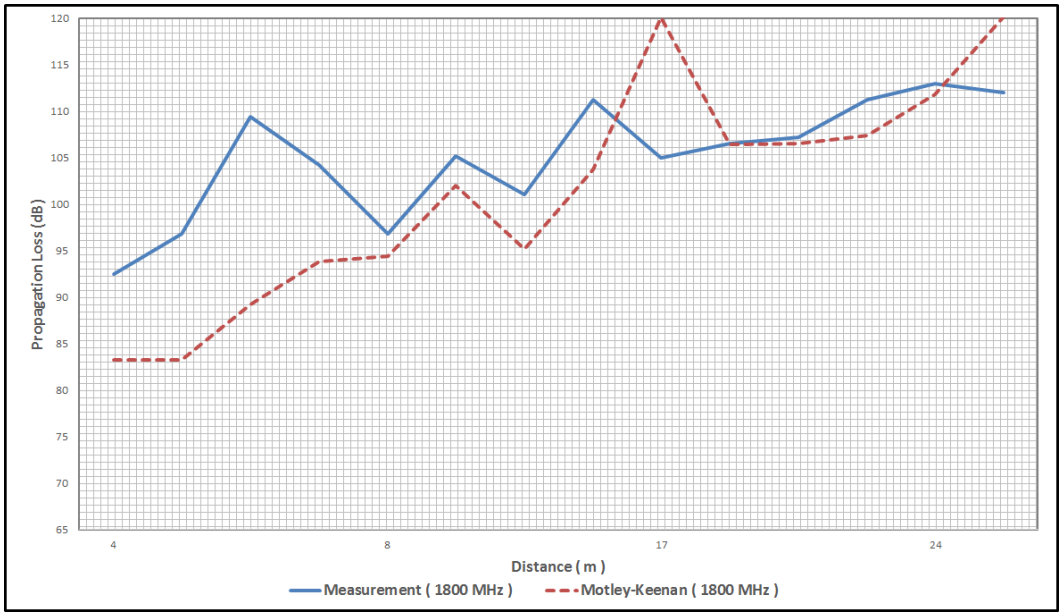

(b)

Figure 3.16. Comparison of Motley-Keenan model and measurement at 1800 MHz, where (a) is for single-floor cases, (b) is for multi-floor cases.

Mean error values for different cases at 1800 MHz are shown in Table 3.12.

Table 3.12. Mean error values for Motley-Keenan model at 1800 MHz.

Case	Mean Error[dB]
Single-Floor	5.7
Multi-Floor	7.2
LOS	4.0
Light Obstruction	5.9
Heavy Obstruction	6.4

Results of Motley-Keenan model are close to that of Single-Slope model with slightly improved LOS prediction and slightly worsened obstructed path loss. Motley-Keenan model's data fits slightly better to actual measurement data in the graphs compared to Single-Slope model. For multi-floor scenarios, use of 40 dB floor loss presents better results than Single-Slope model. The main problem with Motley-Keenan model is that it is hard to predict number of walls in each scenario. Many scenarios include obstructing materials of different width and different type. Entering correct n_w value is not an easy task and requires many simplifications which could lead to excessive errors. Another thing is that use of $a_w = 7$ could vary from place to place as it represents an average concrete wall loss.

3.2.6. Improved Motley Keenan Model

Improved Motley-Keenan model aims to improve the accuracy of the standard model by introducing wall thickness into equation. Also, the model tries to address the uncertainity of wall attenuation problem by tying it to some reference values in the literature. Reference wall loss parameters in Section 2.6 are used. Our office environment consists mostly of rooms seperated by plaster walls and main concrete walls seperating north and south of the office building. Plaster walls in the office are measured to be 15 cm thick. Concrete walls are also predicted to be around 15

cm. Same N and L_0 values with standard Motley-Keenan model are used. Improved Motley-Keenan model does not have additional factor for floor loss. In order to account for floor loss, 1.5 m concrete wall seperating the floors is added as another wall type. 20 cm thick concrete with 12 dB and 15 dB reference losses for 900 MHz and 1800 MHz in [24] is used for this new wall type.

Comparison of actual measurement loss to propagation loss predicted for the model at 900 MHz is shown in Figure 3.17.

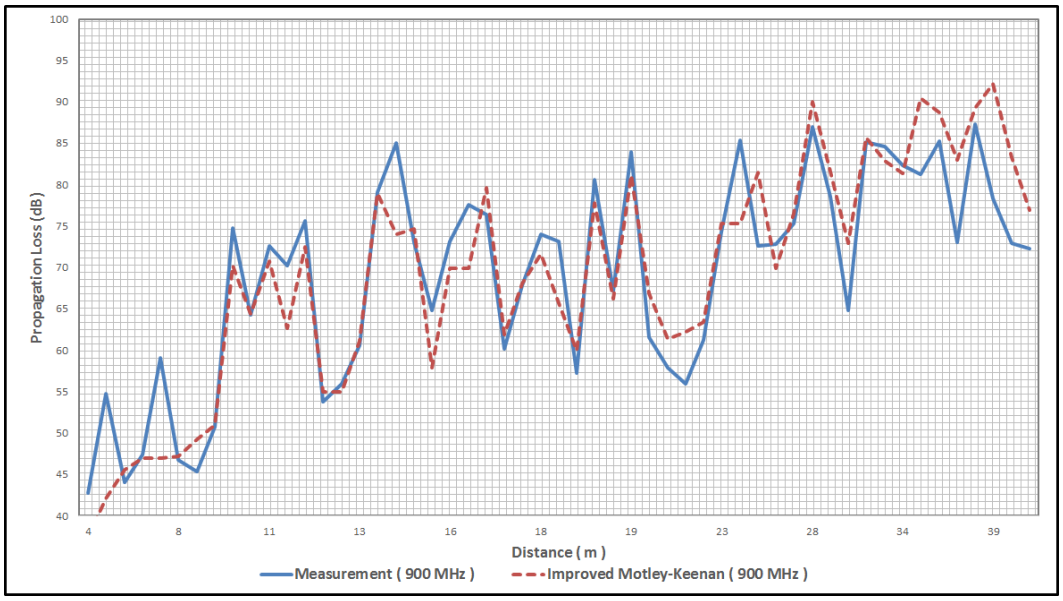

(a)

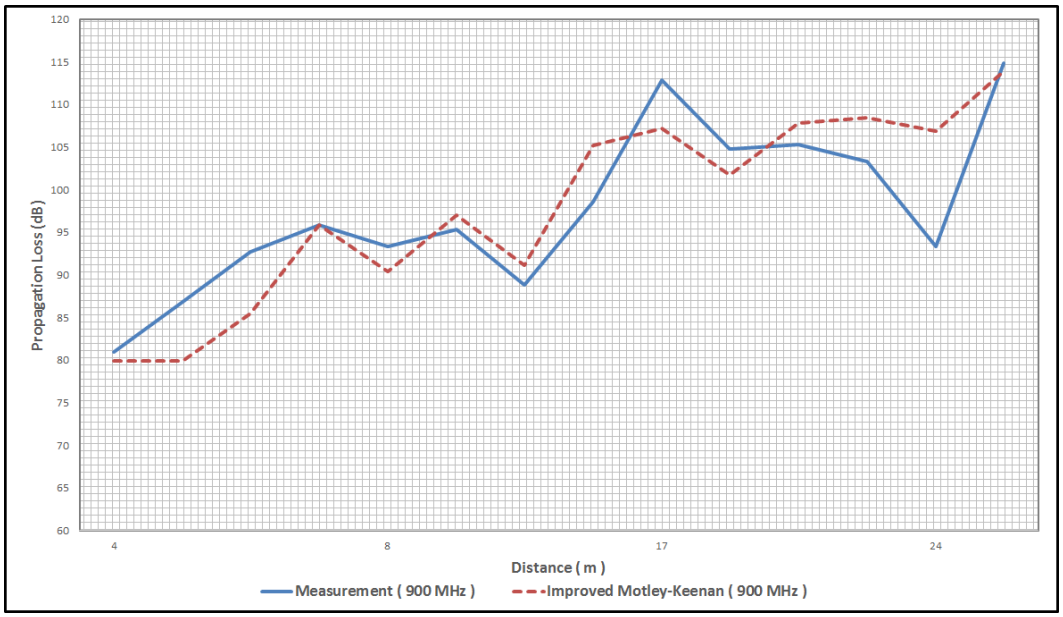

(b)

Figure 3.17. Comparison of Improved Motley-Keenan model and measurement at 900 MHz, where (a) is for single-floor cases, (b) is for multi-floor cases.

Mean error values for different cases at 900 MHz are shown in Table 3.13.

Table 3.13. Mean error values for Improved Motley-Keenan model at 900 MHz.

Case	Mean Error[dB]
Single-Floor	4.2
Multi-Floor	4.3
LOS	2.7
Light Obstruction	5.9
Heavy Obstruction	4.3

Comparison of actual measurement loss to propagation loss predicted for the model at 1800 MHz is shown in Figure 3.18.

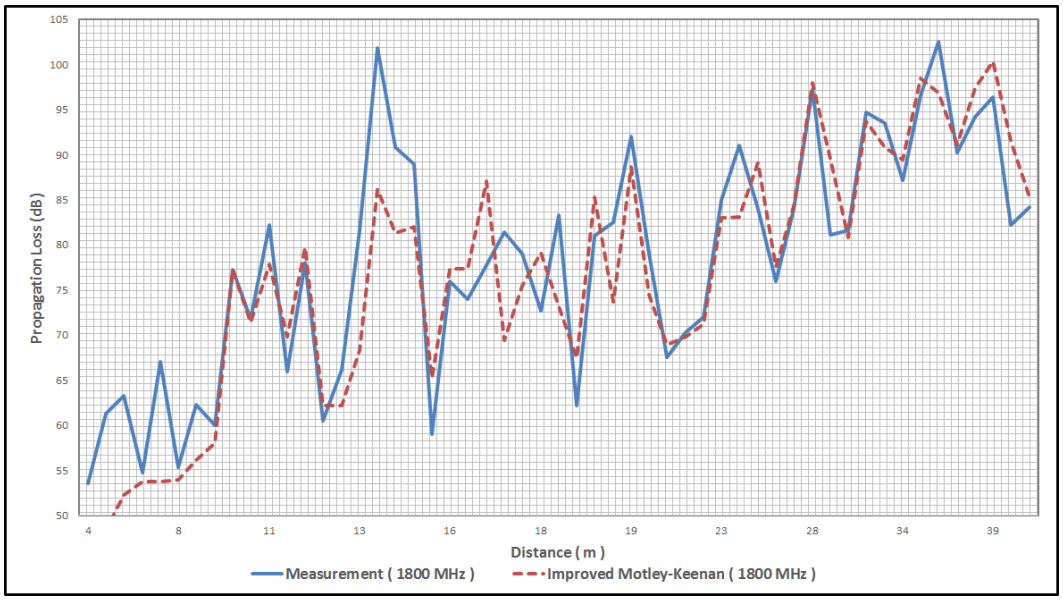

(a)

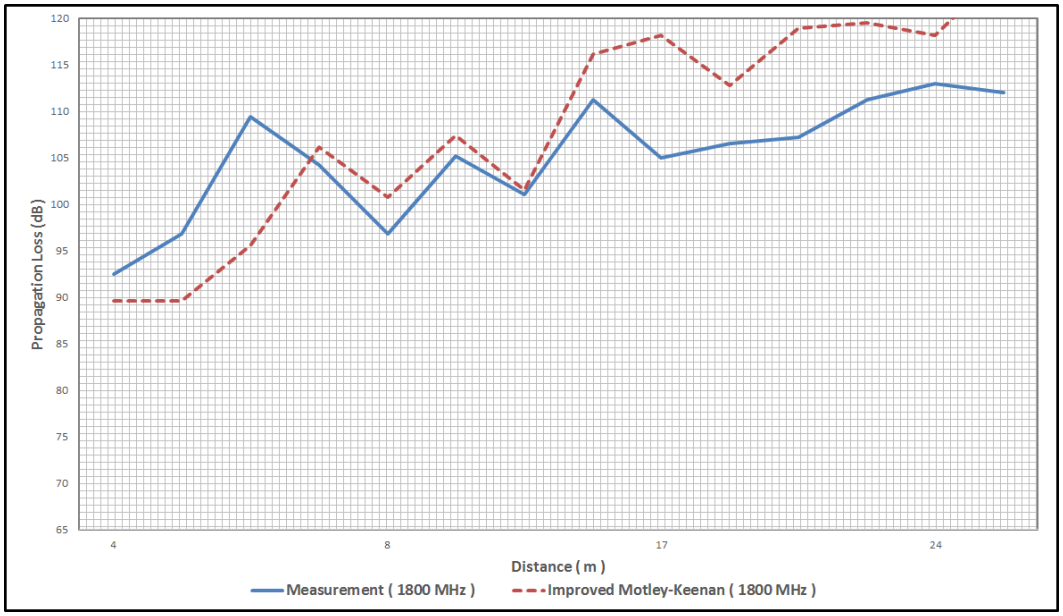

(b)

Figure 3.18. Comparison of Motley-Keenan model and measurement at 1800 MHz, where (a) is for single-floor cases, (b) is for multi-floor cases.

Mean error values for different cases at 1800 MHz are shown in Table 3.14.

Table 3.14. Mean error values for Improved Motley-Keenan model at 1800 MHz.

Case	Mean Error[dB]
Single-Floor	4.9
Multi-Floor	6.8
LOS	4.0
Light Obstruction	8.5
Heavy Obstruction	4.2

Improved Motley-Keenan model increases the accuracy of standard model by introducing wall thickness. The superiority of this model is that it removes the need to prior knowledge of wall loss factor. Only knowledge required is the width of walls in the measurement area and some reference wall loss values which are abundant in the literature. Floor loss prediction also gave close results with a mean error of 4.3 and 6.8. This justifies modeling of the floor as an additional wall.

3.2.7. Akerberg Model

Akerberg model gives maximum and minimum values for path loss depending on distance. Average of maximum and minimum values are taken to predict a single value.

Comparison of actual measurement loss to propagation loss predicted for the model at 900 MHz is shown in Figure 3.19.

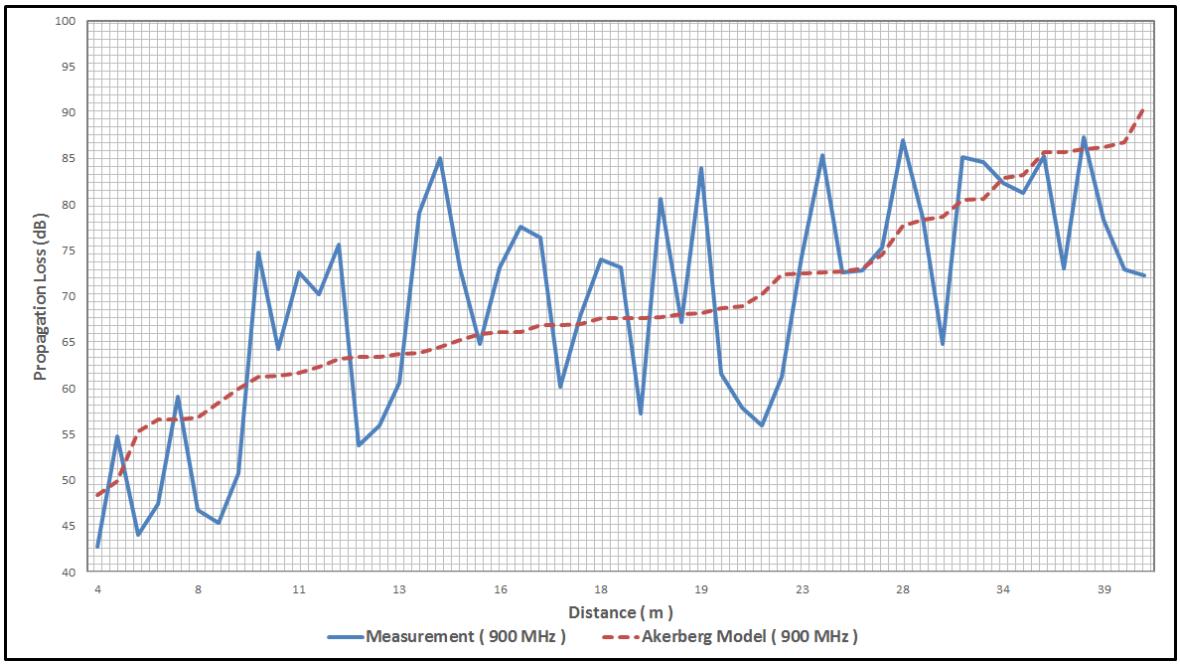

Figure 3.19. Comparison of Akberberg model and measurement at 900 MHz for single-floor cases.

Mean error values for different cases at 900 MHz are shown in Table 3.15.

Table 3.15. Mean error values for Akerberg model at 900 MHz.

Case	Mean Error[dB]
Single-Floor	7.8
Multi-Floor	36.2
LOS	9.5
Light Obstruction	7
Heavy Obstruction	7.3

Comparison of actual measurement loss to propagation loss predicted for the model at 1800 MHz is shown in Figure 3.20.

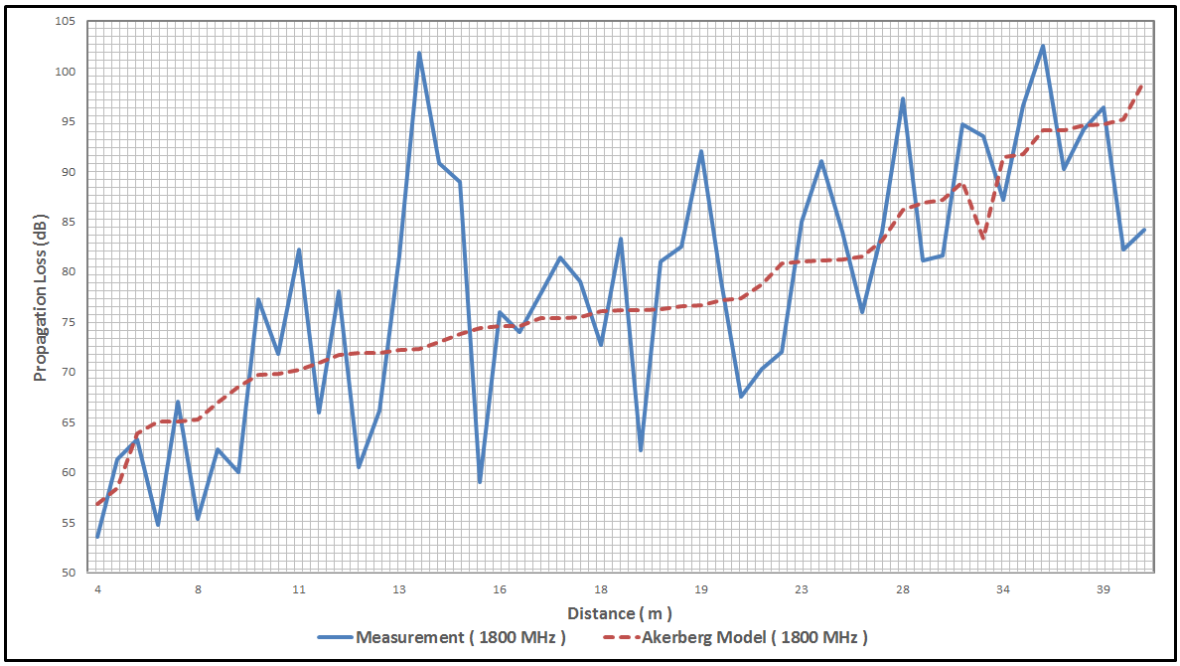

Figure 3.20. Comparison of Akberberg model and measurement at 1800 MHz for single-floor cases.

Mean error values for different cases at 1800 MHz are shown in Table 3.16.

Table 3.16. Mean error values for Akerberg model at 1800 MHz.

Case	Mean Error[dB]
Single-Floor	7.3
Multi-Floor	35.2
LOS	8.5
Light Obstruction	6.2
Heavy Obstruction	7.1

Akerberg model provides similar results with ITU-R model. The model does not provide a way to include floor loss into equation and because of this multi-floor predictions are far-off.

3.2.8. Multi-Wall Model

Multi-Wall model adds wall losses, floor losses and a constant loss to free space loss. For wall attenuation, light wall and heavy wall loss parameters provided by the model in [8] are used. For floor loss, value of 18.3 dB per floor is provided. As we assumed each floor wall of NETAS office acts like two floors, twice the value is used as floor attenuation factor. In floor map, plaster walls are counted as light walls and concrete walls are counted as heavy walls. Some dense or metallic obstructions like servers, shelves and elevator shaft are also counted as heavy walls.

Comparison of actual measurement loss to propagation loss predicted for the model at 900 MHz is shown in Figure 3.21.

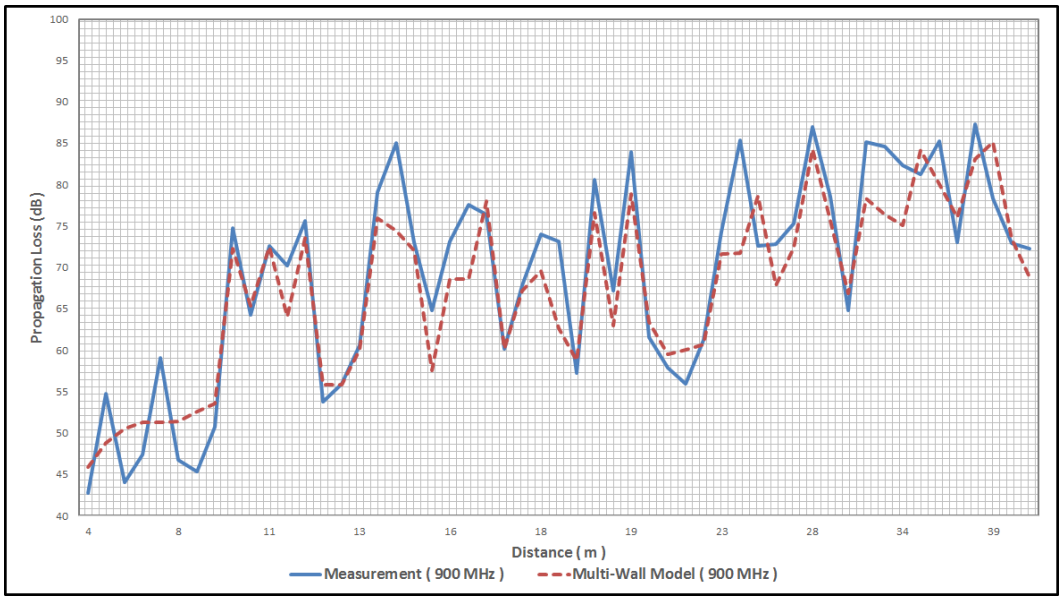

(a)

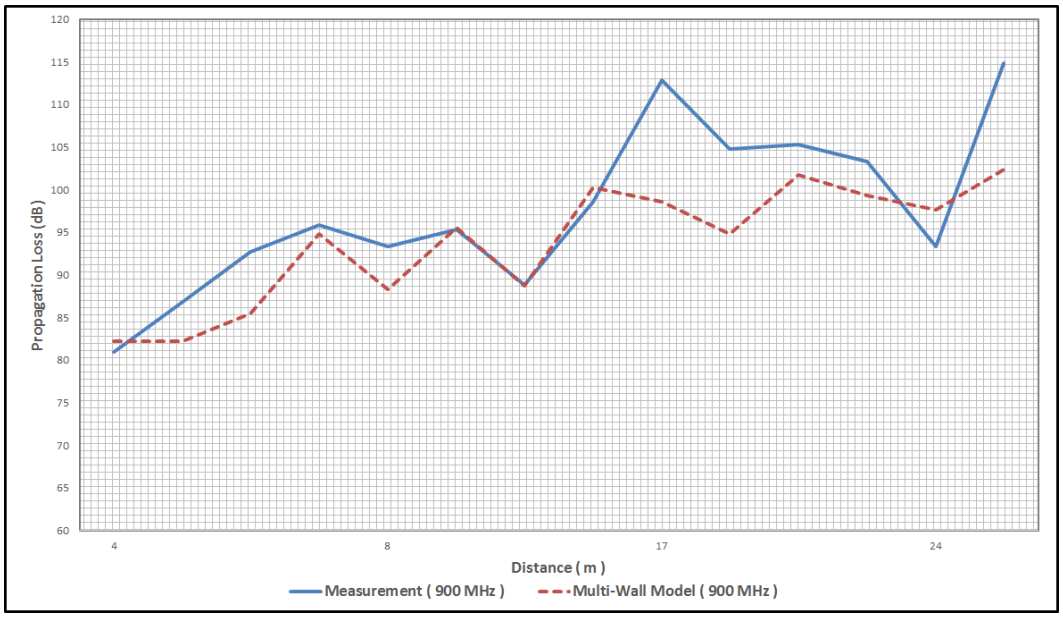

(b)

Figure 3.21. Comparison of Multi-Wall model and measurement at 900 MHz, where (a) is for single-floor cases, (b) is for multi-floor cases.

Mean error values for different cases at 900 MHz are shown in Table 3.17.

Table 3.17. Mean error values for Multi-Wall model at 900 MHz.

Case	Mean Error[dB]
Single-Floor	4.1
Multi-Floor	5.0
LOS	3.5
Light Obstruction	4.0
Heavy Obstruction	4.4

Comparison of actual measurement loss to propagation loss predicted for the model at 1800 MHz is shown in Figure 3.22.

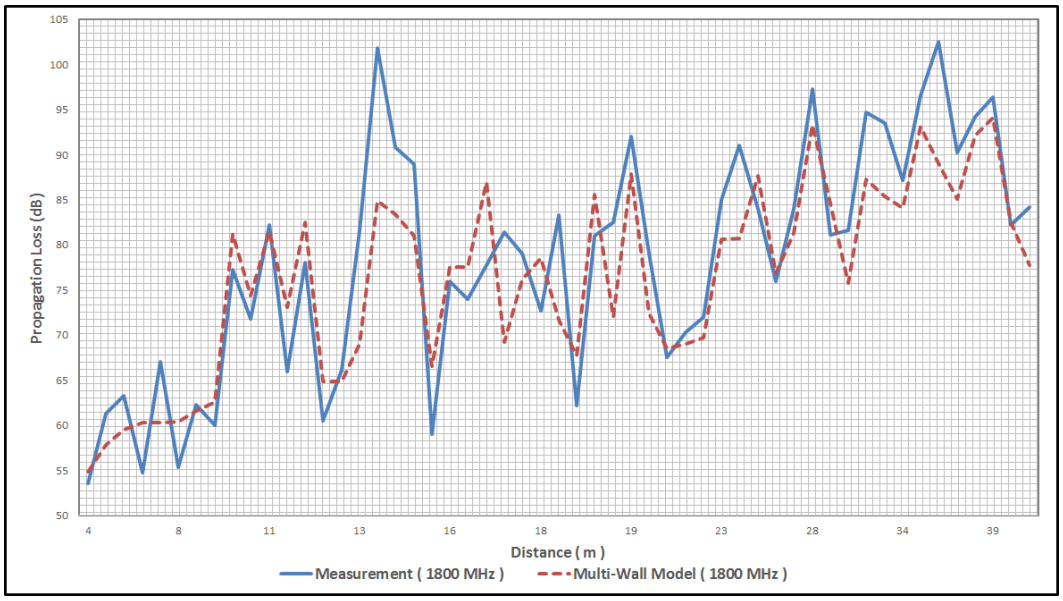

(a)

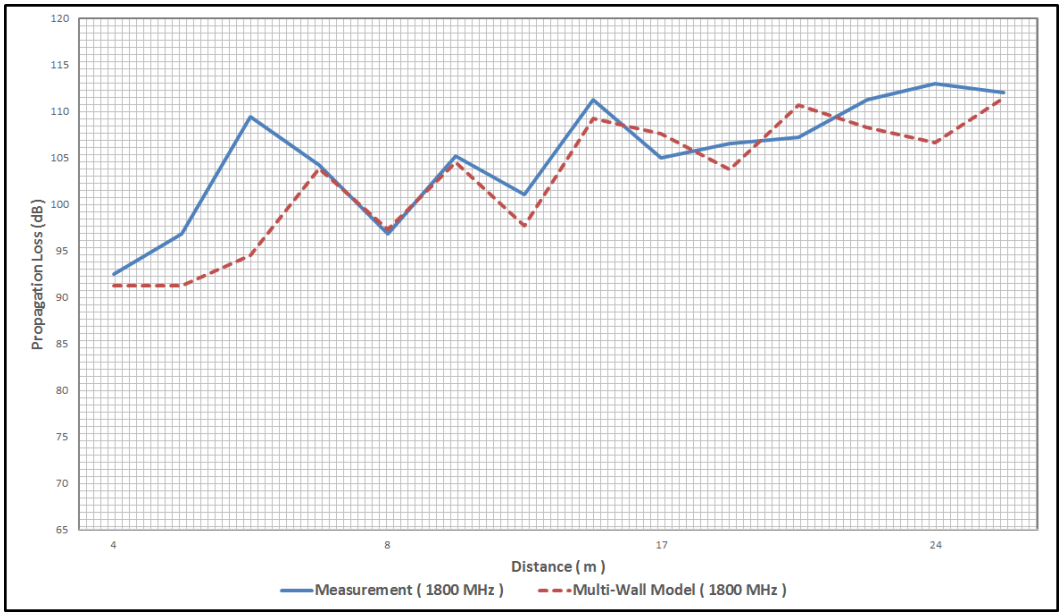

(b)

Figure 3.22. Comparison of Multi-Wall model and measurement at 1800 MHz, where (a) is for single-floor cases, (b) is for multi-floor cases.

Mean error values for different cases at 1800 MHz are shown in Table 3.18.

Table 3.18. Mean error values for Multi-Wall model at 1800 MHz.

Case	Mean Error[dB]
Single-Floor	5.2
Multi-Floor	3.4
LOS	3.2
Light Obstruction	8.4
Heavy Obstruction	5.1

Multi-Wall model achieves good accuracy for both single-floor and multi-floor scenarios. Performance is close to Improved Motley-Keenan model with the requirement of fewer input parameters. Multi-Wall model does not use different path loss exponent, instead L_c, a constant loss is added. L_c value is found to be 2 and 5 for 900 MHz and 1800 MHz respectively in our office.

3.2.9. Winner II Model

Winner-II model is developed for 2-5 GHz range. Similar to Single-Slope model, it provides different path loss exponent, constant loss and wall attenuation values for several scenarios. Because of its frequency range, only 1800 MHz measurements were implemented with this model.

Comparison of actual measurement loss to propagation loss predicted for the model at 1800 MHz is shown in Figure 3.23.

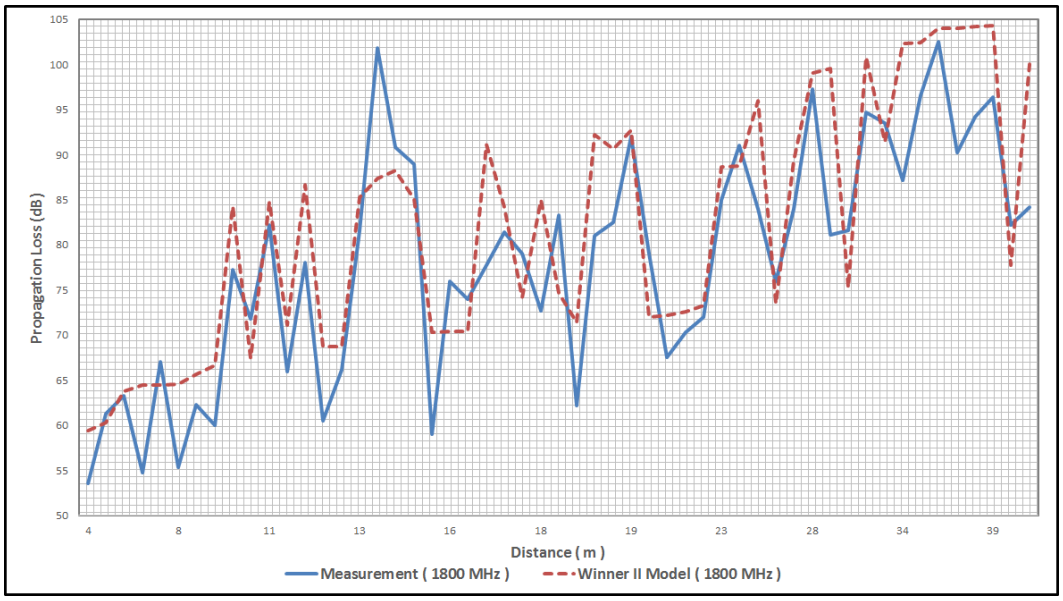

(a)

(b)

Figure 3.23. Comparison of Winner II model and measurement at 1800 MHz, where (a) is for single-floor cases, (b) is for multi-floor cases.

Mean error values for different cases at 1800 MHz are shown in Table 3.19.

Table 3.19. Mean error values for Winner II model at 1800 MHz.

Case	Mean Error[dB]
Single-Floor	6.5
Multi-Floor	15.1
LOS	5.7
Light Obstruction	6.2
Heavy Obstruction	6.9

Multi-floor performance of Winner II is not good despite usual two-floor assumption. The reason for this is that similar to ITU-R model floor loss equation for Winner II model predicts only 4 dB increase in loss after the first floor. This is not compatible with measurement results.

3.2.10. Lecours Model

Similar to Multi-Wall model, Lecours model adds excessive loss over free space loss. Additional loss factors for wall attenuation, floor attenuation, diffraction, reflection and furniture effect are added. Additional wall attenuation is a distance dependent parameter suggested for 900 MHz. Due to this, only 900 MHz implementation of the model was done.

Comparison of actual measurement loss to propagation loss predicted for the model at 900 MHz is shown in Figure 3.24.

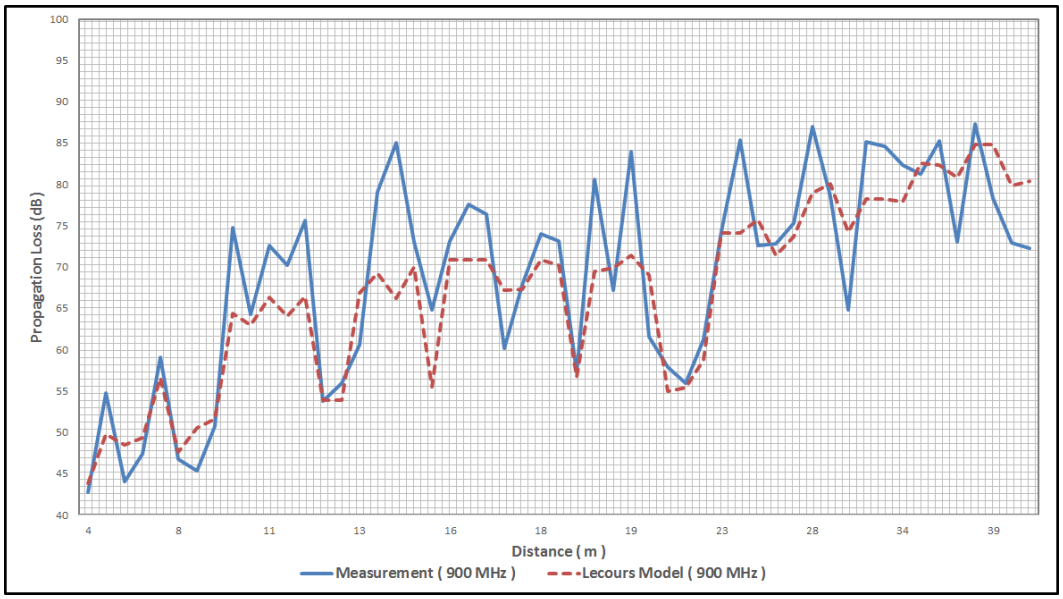

(a)

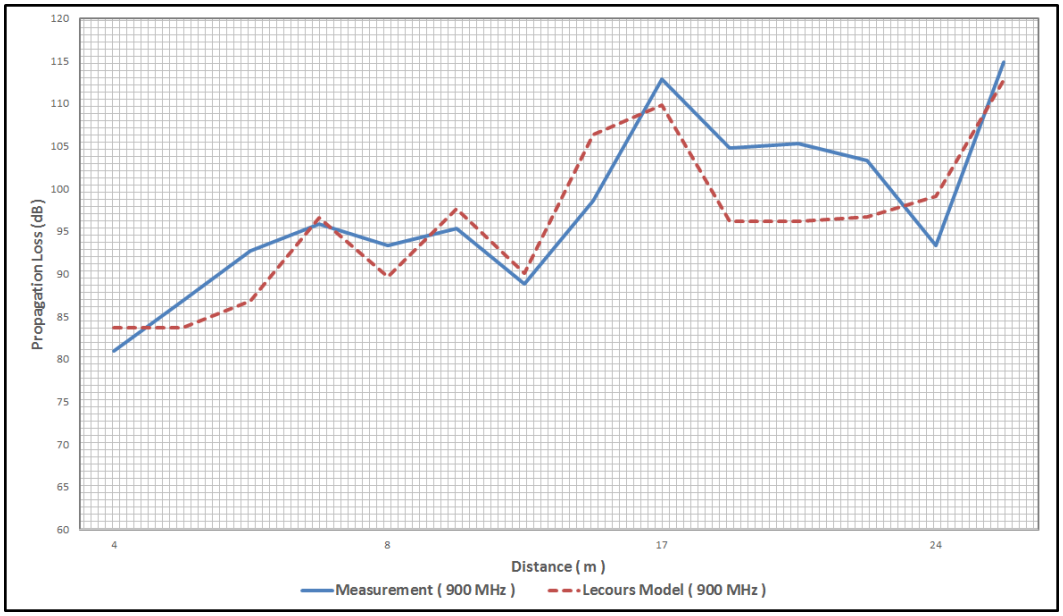

(b)

Figure 3.24. Comparison of Lecours model and measurement at 900 MHz, where (a) is for single-floor cases, (b) is for multi-floor cases.

Mean error values for different cases at 900 MHz are shown in Table 3.20.

Table 3.20. Mean error values for Lecours model at 900 MHz.

Case	Mean Error[dB]
Single-Floor	5
Multi-Floor	4.5
LOS	2.5
Light Obstruction	5.7
Heavy Obstruction	5.8

Attenuation of a single wall predicted by the model seems to be higher than loss of our plaster walls. Plaster walls are counted as thin walls and as suggested in the model each of them are taken as 1/2 wall. Reflection addition for corridors improved few cases that suits it. For floor attenuation, attenuation for two floors which yields 40 dB is used. Diffraction formula of the model resulted in good correction for corners. Although good accuracy for both single-floor and multi-floor scenarios are achieved, single wall attenuation formula causes frequent undershoots in scenarios with many obstructions.

3.2.11. Reduced Complexity UTD Indoor Model

UTD Indoor Model has two slopes like Dual-Slope Model, wall attenuation approach of Multi-Wall model with incidence angle addition and diffraction parameter. The model was implemented for only 900 MHz as [20] provided parameters for only this frequency.

Comparison of actual measurement loss to propagation loss predicted for the model at 900 MHz is shown in Figure 3.25.

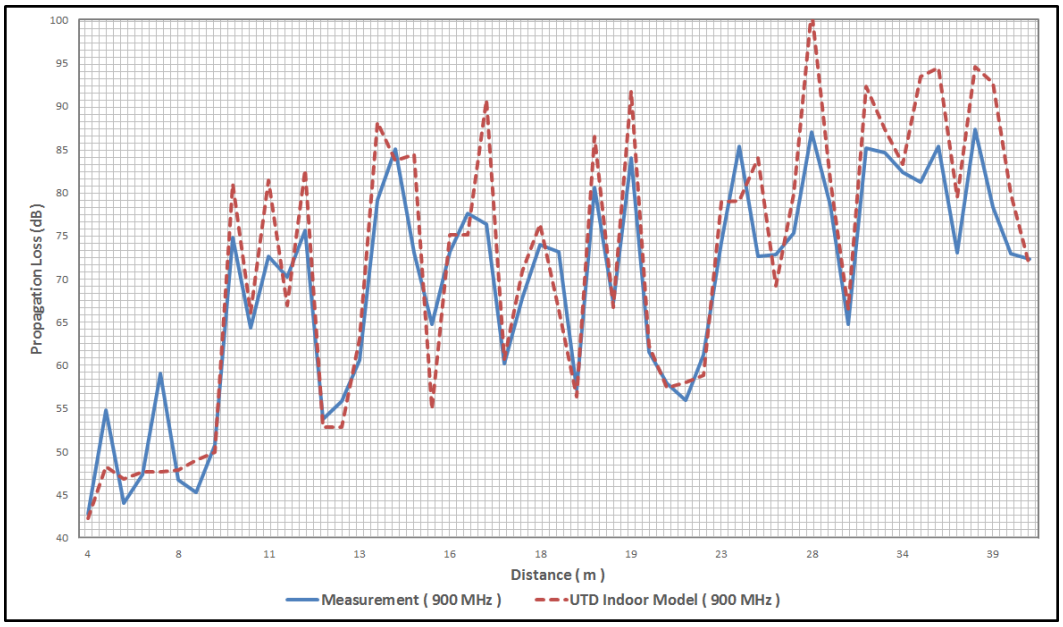

(a)

(b)

Figure 3.25. Comparison of UTD Indoor model and measurement at 900 MHz, where (a) is for single-floor cases, (b) is for multi-floor cases.

Mean error values for different cases at 900 MHz are shown in in Table 3.21.

Table 3.21. Mean error values for UTD Indoor model at 900 MHz.

Case	Mean Error[dB]
Single-Floor	4.9
Multi-Floor	4.4
LOS	2.2
Light Obstruction	3.5
Heavy Obstruction	6.5

UTD indoor model performed somewhat worse than Multi-Wall model. This is due to high heavy wall attenuation numbers given for the model. This created a lot of overshoots in the model which significantly increased mean absolute error. LOS propagation yielded very accurate results because of two-slopes used in this model.

Diffraction addition fixed several overshoots for corridor corners and rooms with windows. Angle of incidence for walls made small positive addition. Angle of incidence for floor penetration made no observable difference.

3.3. Comparison of Models

Improved Motley-Keenan and Multi-Wall models presented best predictions for both 900 and 1800 MHz. Multi-Wall model outperformed Improved Motley-Keenan model by a slim margin at 900 MHz. Improved Motley-Keenan did the same at 1800 MHz with a bigger margin.

Addition of explicit wall attenuation significantly improved accuracy. Our test environment included lots of plaster walls, glass partititons and conrete walls. Changing path loss exponent for different obstruction densities (as Single-Slope or Winner II models do) is less accurate than explicit addition of wall attenuations. Number of wall types and different attenuation factors for them also increased performance. Multi-Wall

model which used two-wall types (heavy and light) gave better results than Motley-Keenan model which has only one wall type.

Multi-Wall model which is one of the best two models use free-space loss of 20. Additional L_c factor of 2 dB and 5 dB is added in this model to approximate path loss shift. The other best model Improved Motley-Keenan model used path loss exponent of 35. So, the path loss exponent is expected to be in the range of 20 to 35.

Floor attenuation did not work as expected. Seperation by a single floor dropped signal levels much more than that is predicted by any models. Measurements showed that 1.5 m thick steel-reinforced floor wall of NETAS office acted like two floors seperation. As a result, floor number of 2 is used for all of the models and accurate results obtained from several models.

Different path loss slope was observed in the near vicinity of transmitter. Adding second-slope to Improved Motley-Keenan model for example gives more accurate predictions in the close range. This effect could be observed by comparing the graphs of Improved Motley-Keenan model and Optimized model that is suggested in the next chapter.

Simplified UTD diffraction produced good results, especially for corridor corners. However, the effort for this method is quite a lot. Taking angle of incidence account for walls into account improved predictions. This becomes more observable after around 50 degrees.

Through-wall physical model is used to estimate wall attenuation factors for concrete walls, plaster walls and glass partitions in NETAS office. The values found using this method are compared to the similar reference values in the literature. Traversing effect mentioned in Multi-Wall-and-Floor model is also tested along with Through-wall physical model. For second traversed wall, 1 dB reduction in path loss is observed though this observation could be due to measurement error margins.

4. OPTIMIZED PROPAGATION MODEL

Indoor propagation models in the literature are evaluated and compared with measurement results in Chapter 3. Strong and weak sides of different models are shown. In this section, based on the results from the previous section, the following hybrid propagation model is suggested,

$$L_F(d) = \begin{cases} L(d) & \text{Direct,} \\ -10\log\left[l(d_c)l(d_{c'}) \times |D(d_c,\phi_c,d'_c,\phi'_c)|^2 + l(d)\right] & \text{Direct+Diffraction,} \\ 32.1 - 20\log|R_n| - 20\log\left[\frac{1-[R_n]^2}{1+[R_n]^2}\right] + 17.8\log d + & \\ 8.6\left[-\ln|R_n|(\frac{\pi n}{h})\frac{d}{p_n^{(0)}h}\right] & \text{Waveguide,} \end{cases} \tag{4.1}$$

where d is the direct distance between transmitter and receiver, d_c is the distance between diffracting corner and receiver, d'_c is the distance between diffracting corner and transmitter, ϕ_c is the angle between diffracting corner and receiver, ϕ'_c is the angle between diffracting corner and transmitter, $D(d_c,\phi_c,d'_c,\phi'_c)$ is diffraction parameter, $L(d)$ is path loss formula for direct path, $l(.) = 10^{-L(.)/10}$, h is the height of corridor, k is wavenumber, n is the number of reflections, $p_n^{(0)} = \sqrt{k^2 + (\pi n/h)^2}$ and R_n is the reflection coefficent of each wall.

4.1. Direct Propagation

Direct propagation is characterized by path loss along the direct route between transmitter and receiver. In the proposed Optimized model, it is denoted as $L(d)$ and is given by,

$$L(d) = L_0 + \sum_{i=1}^{I}\sum_{l=1}^{L_i} L_{0ij}\, 2^{\log_3 \frac{e_{il}}{e_{0i}}} / \cos\theta_l + k_f L_f + \begin{cases} N_1 \log_{10} d & 1m < d \le d_{bp}, \\ N_1 \log_{10} d_{bp} + N_2 \log_{10}(\frac{d}{d_{bp}}) & d > d_{bp}, \end{cases} \tag{4.2}$$

where L_0 is the loss at 1m, d is distance, d_{bp} is break-point distance, L_i is number of type i walls, I is number of wall types, L_{0ij} is the penetration loss in type i reference wall for j-th traversed wall, e_{0i} is the thickness of type i reference wall, e_{il} is the thickness of l-th wall of type i, k_f is the number of floors, L_f is floor attenuation factor, θ_l is angle of incidence between l-th wall and direct path between transmitter

and receiver, N_1 is path loss exponent for LOS region and N_2 is path loss exponent for NLOS region.

Based on the measurement results in Chapter 3, path loss formula for direct transmission considering the following effects is suggested.

- Dual Slope: Slope change is observed at around 10 m from transmitter.
- Traversing: The propagation loss for the first traversed wall is greater than the incremental attenuation caused by each additional wall. In order to model this factor, different wall loss factors are used depending on the traversing number.
- Multi-Wall Types: Including different attenuation factors for different walls improved accuracy.
- Angle of Incidence: Anything other than normal incidence would cause additional loss. In order to model this factor, angle of incidence between transmitter and the obstructing wall is added.
- Wall Thickness: In a typical office environment, there are several different types of walls and same type of walls don't have same thickness all over the place. Adding thickness factor into account improves accuracy.

4.1.1. Dual-Slope

It is observed in our measurements that a significant change of slope occurs at 10 m. For this reason, a different path loss exponent is added for cases with range less than 10 m. This new path loss exponent models both LOS to NLOS transition and near-field behaviour of electromagnetic propagation.

Importance of dual-slope approach is seen by comparing LOS scenario results of Dual-Slope model and UTD indoor model to other models. These two models use dual-slopes and gave best LOS case predictions. Because of this, dual-slope approcah

is added to Optimized model. The factor in Equation 4.3 represents this effect.

$$\text{Dual-Slope} = \begin{cases} N_1 \log_{10} d & 1m < d \leq d_{bp}, \\ N_1 \log_{10} d_{bp} + N_2 \log_{10}(\frac{d}{d_{bp}}) & d > d_{bp}. \end{cases} \tag{4.3}$$

4.1.2. Traversing

Multi-Wall-and-Floor Model in [17] provides decreasing wall attenuation values for each successive wall. Our measurements in Section 2.13 also found 1 dB decrease in wall attenuation for the second wall. Therefore, this practical result is integrated to Optimized result with only one level of traversing taken into consideration.

4.1.3. Multi-Wall Types

Using different wall attenuation factors for different valls improved the accuracy as shown in the results of Multi-Wall model.

4.1.4. Angle of Incidence

Through-Wall Physical model showed that transmission coefficient through a wall depends on the angle incidence with 2.24 and 2.25 being the respective formulas. Furthermore, variation of received power with angle of incidence for propagation through concrete walls is provided in [22] and is shown in Figure 2.9. UTD indoor model represents this effect by dividing the wall attenuation by cosine of angle of incidence. It could be argued that received power in Figure 2.9 displays a behaviour similar to cosinusoidal decay. The conclusion is that the approach in UTD indoor model is both reasonable and easy to use. As a consequence, angle of incidence modeling in UTD indoor model is integrated to Optimized model.

4.1.5. Wall Thickness

When a propagation prediction is to be made in an indoor environment, reference wall losses for different obstructing materials are assumed. However, depending on the thickness of these materials, assumed values from the literature may not fit actual loss values because of major differences in obstruction width.

Improved Motley-Keenan model introduced wall thickness into equation and the results show that considerable increase in accuracy is achieved over standard model with this approach. Improved Motley-Keenan approach requires the knowledge of attenuation and thickness value for some reference obstructions. On the other hand, standard Motley-Keenan model requires the assumption of some reference attenuation values for the walls. This could be problematic because in the literature, wall attenuation values are given with two terms; attenuation and thickness. Standard model has to choose some average value reflecting the test environment and this could result in substantial differences between actual value and assumed one. Because of superior performance of Improved Motley-Keenan model over standard model, wall thickness in this model is integrated to Optimized model. The following factor in Equation 4.4 accounts for the effects of multi-walls, traversing, wall thickness and angle of incidence and is given by,

$$\text{Thickness/Multi-Wall/Angle/Traversing} = \sum_{i=1}^{I} \sum_{l=1}^{L_i} L_{0ij} 2^{\log_3 \frac{e_i l}{e_{0i}}} / \cos\theta_l. \qquad (4.4)$$

Equation 4.4 includes combined effects of multi-wall, thickness, angle of incidence and traversing.

Division of the wall attenuation with $\cos\theta_l$ reflects approximation of angle's effect on transmission coefficient. This behaviour is confirmed in both [20] and [22].

Dependence of reference attenuation value L_{0ij} on the number of traversed walls

are confirmed in both our Through-Wall Physical model measurements and in [17].

Improved Motley-Keenan's model's thickness conversion factor which is expressed as $\sum_{l=1}^{L_i} L_{0ij} 2^{\log_3 \frac{e_i l}{e_{0i}}}$ is included in Equation 4.3.

Multi-wall effect is included by factor $\sum_{i=1}^{I}$ where i represents the number of different wall types.

4.2. Diffraction

To model diffraction from corridor corners, diffraction approach in UTD indoor model is integrated to Optimized model. Unlike UTD indoor model, only diffraction from one corner is included in the model. In order to calculate diffraction coefficient $D(d, \phi, d', \phi')$ necessary for the model, UTD has to be used. Implementation of UTD for corridors with corners are shown in [25]. Computational effort of UTD is however too much for quick signal level prediction. Luebber introduced heuristic diffraction coefficient (LHDC) in [26] which provides a computationally efficient modification to the UTD equations. The problem with Luebbers heuristic diffraction coefficient (LHDC) is that it is small in the region between the two shadow boundaries, and that it has a deep null in the illuminated region that does not appear to have a physical basis. As a result, amplitude predictions made by using the LHDC in the aforementioned regions are low. New heuristic diffraction coefficient (NHDC) equations in [27] are suggested to overcome the mentioned problems of Luebbber's approach. In optimized model, UTD equations for wedges in [27] are used.

Wedge diffraction in UTD is shown in Figure 4.1. The diffracted electric field is given in Equation 4.5 [27],

$$E_{diff} = E_i D(\phi, \phi') \sqrt{\frac{\rho'}{\rho(\rho + \rho')}} e^{-jk\rho}, \tag{4.5}$$

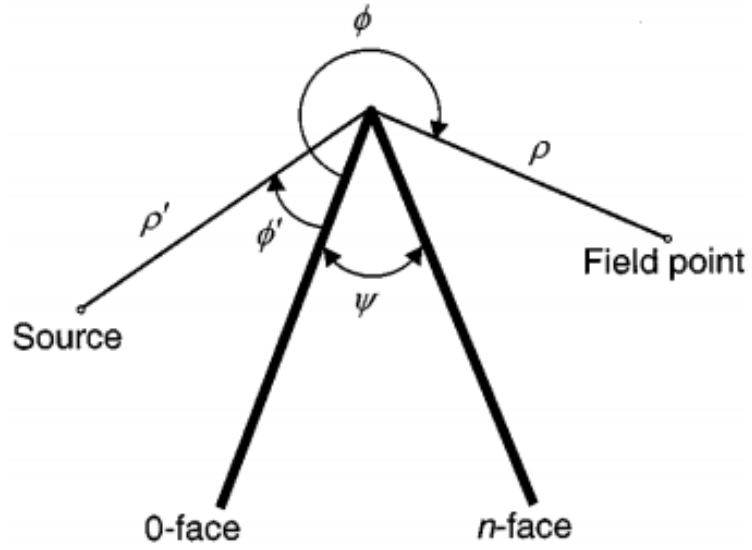

Figure 4.1. Wedge Diffraction in UTD.

where $D(\phi, \phi')$ is UTD diffraction coefficient used in Equation 4.1 and is given by,

$$D(\phi,\phi') = -\frac{1}{\sqrt{2\pi k}} \times \begin{pmatrix} (\pi - |\phi - \phi'|)^{-1} \cdot F[kLa^{-}(\phi - \phi')] \\ +(\pi + |\phi - \phi'|)^{-1} \cdot F[kLa^{+}(\phi - \phi')] \end{pmatrix}, \tag{4.6}$$

where k is the wavenumber, $F(kLa^{\pm}(\phi - \phi'))$ is *transition* function, L is a distance parameter and $a^{\pm}$ is a measure of the angular separation between the field point and a shadow or reflection boundary. Formulas to calculate $F(kLa^{\pm}(\phi - \phi'))$, L and $a^{\pm}$ are given in [21] and [26].

As the divergence factor in terms of power $\left(\frac{\rho'}{\rho(\rho+\rho')}\right)$ effectively gives a path loss exponent of 10 when receiver is near diffracting point ($\rho < d_{bp}$), $N_1 = 10$ is used in Equation 4.2 for diffracted fields. For $\rho > d_{bp}$, the original N_2 value specified is used.

4.3. Waveguide Propagation

For long hallways, direct propagation calculations predicts higher path loss than actual value. This is due to waveguiding effect of corridors. Waveguide model for

corridors are suggested in [28] and [29] to calculate path loss in halways. In these works, hallways are considered as slab waveguides. Geometry of waveguide propagation is shown in Figure 4.2.

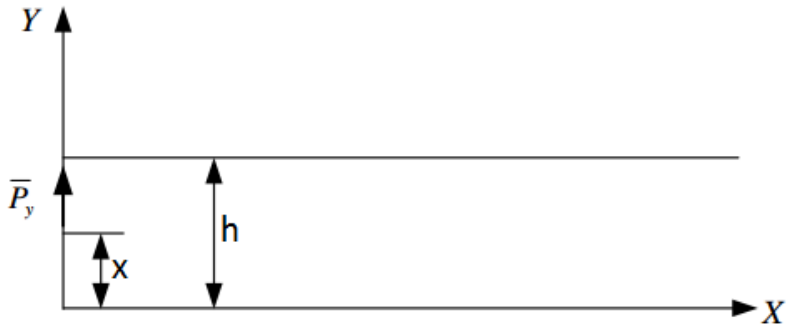

Figure 4.2. Corridor waveguide model.

As $h \gg \lambda$ where h is the corridors width and λ is then wavelength, approximation of geometrical theory of diffraction (UTD) is used in [29]. This approximation is valid as long as the first Fresnel zone $\sim (\lambda d)^{1/2}$, equals or does not exceed the width of corridor h.

The electrical properties of walls are described by the wave impedance Z_{EM} given by,

$$Z_{EM} = \frac{1}{\sqrt{\epsilon}}, \tag{4.7}$$

where $\epsilon = \epsilon_0 - j(4\pi\sigma/w)$.

Reflection coefficent of the walls is given by,

$$R_n = \frac{K_n - kZ_{EM}}{K_n + kZ_{EM}}, \tag{4.8}$$

where $K_n = \frac{n\pi}{h}$ and $k = \frac{2\pi}{\lambda}$.

The path loss for hallway is then given in [29] by,

$$L = 32.1 - 20\log|R_n| - 20\log\left[\frac{1-[R_n]^2}{1+[R_n]^2}\right] + 17.8\log d + 8.6\left[-\ln|R_n|(\frac{\pi n}{h})\frac{d}{p_n^{(0)}h}\right]. \quad (4.9)$$

For ferroconcrete walls $R_n = 1$ and for brick building walls $\epsilon_r = 15 - 17$, $\sigma = 0.05 - 0.08$ and $0.73 - 0.81$ are suggested in [29].

4.4. Parameters

Parameters for the model are given in Table 4.1.

Table 4.1. Model coefficients for Optimized Model.

Frequency	N_1	N_2	L_0[dB]	L_f[dB]	d_{bp}[m]
900 MHz	20	30	30	40	10
1800 MHz	20	30	38	40	10

For wall losses, the values found in Section 3.2.1 are used with the addition of traversing effect. Reference wall losses at 900 MHz and 1800 MHz are given in Table 4.2 and Table 4.3.

Table 4.2. Reference wall losses at 900 MHz.

Wall Type	Thickness[cm]	j=1	j=2
Glass	1	2	-
Plaster Wall	12	2.5	1.5
Concrete Wall	15	8	7

Table 4.3. Reference wall losses at 1800 MHz.

Wall Type	Thickness[cm]	j=1	j=2
Glass	1	2	-
Plaster Wall	12	3.5	2.5
Concrete Wall	15	9	8

4.5. Results

Implementation of our optimized model to our measurements at 900 MHz and 1800 MHz are shown in Figure 4.3 and Figure 4.4 respectively.

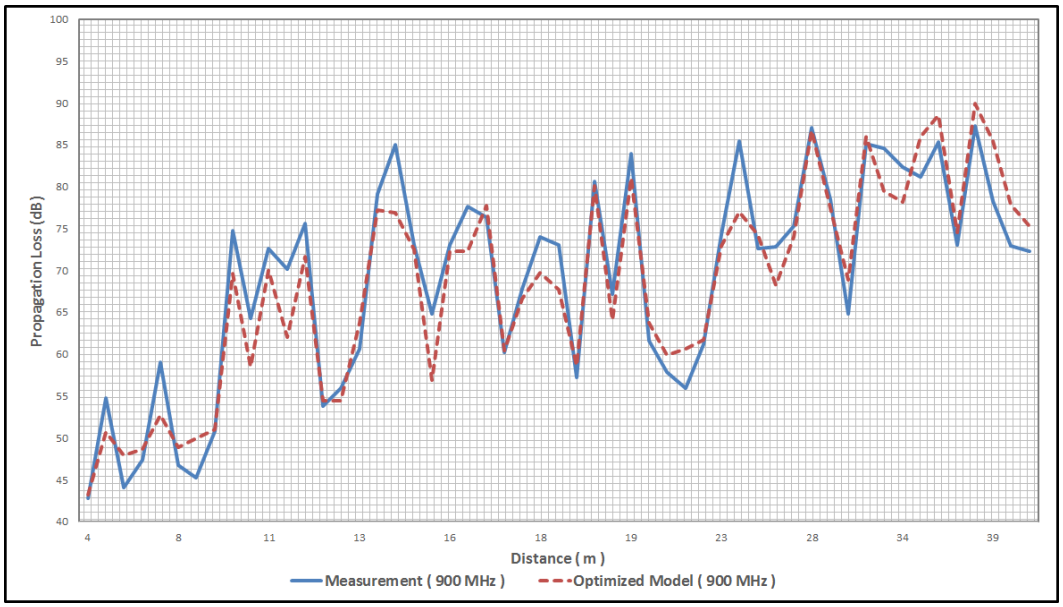

(a)

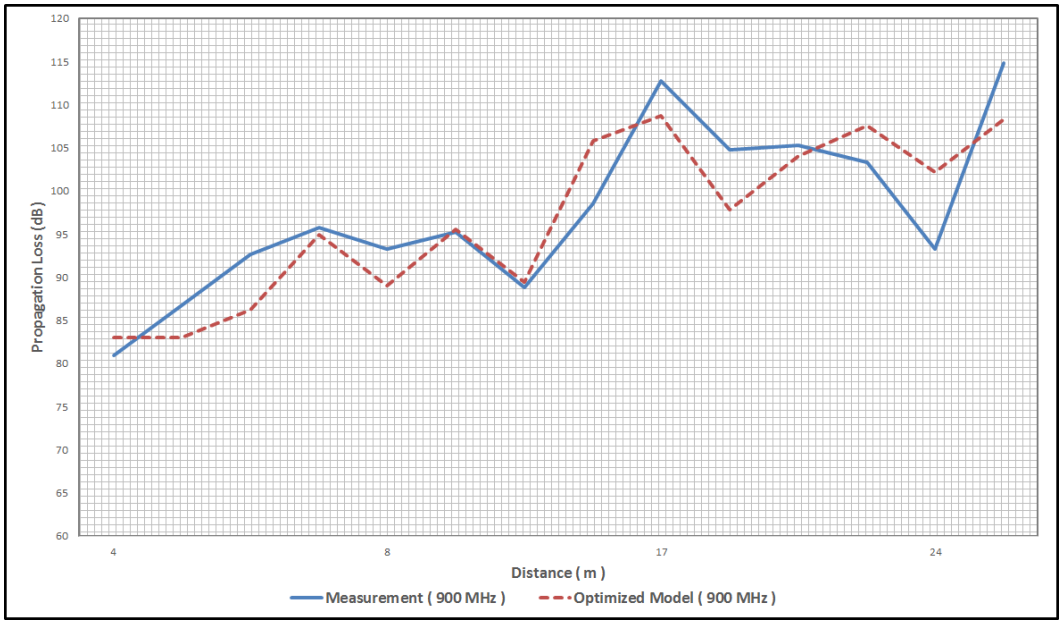

(b)

Figure 4.3. Comparison of Optimized model and measurement at 900 MHz, where (a) is for single-floor cases, (b) is for multi-floor cases.

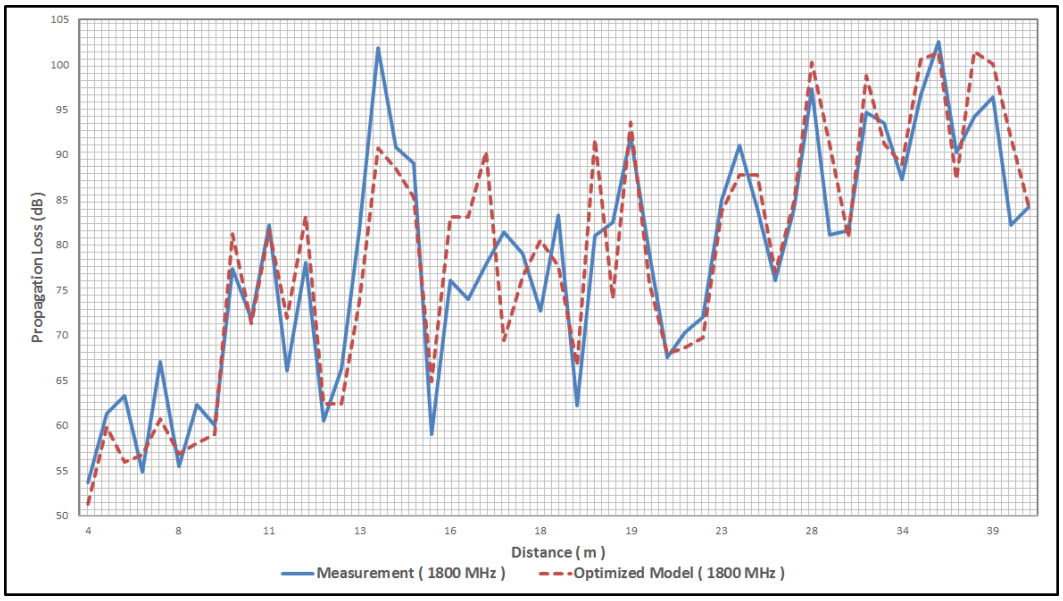

(a)

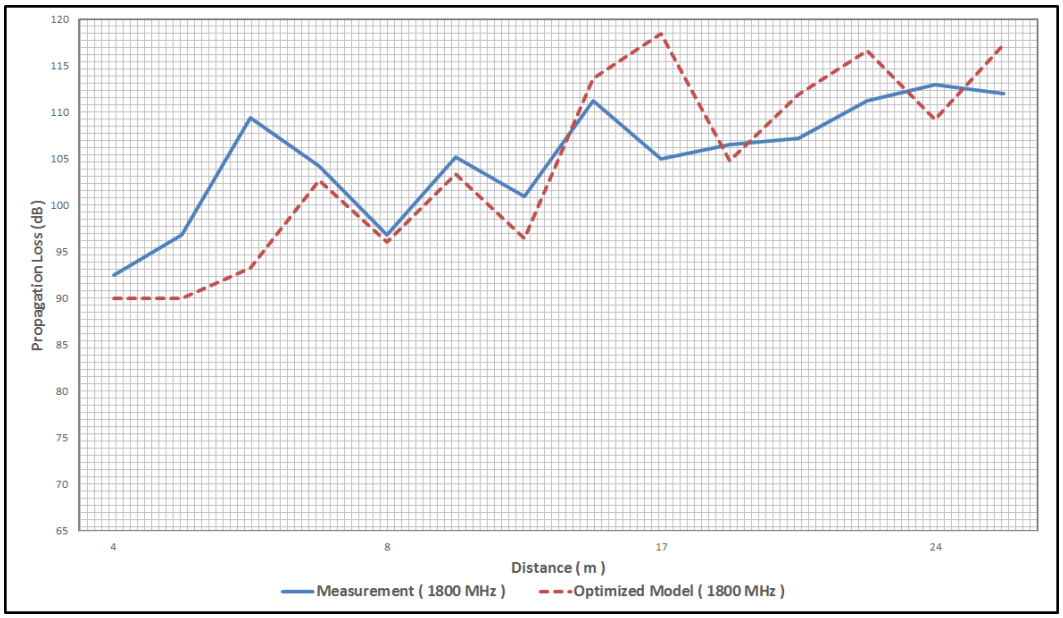

(b)

Figure 4.4. Comparison of Optimized model and measurement at 1800 MHz, where (a) is for single-floor cases, (b) is for multi-floor cases.

As seen from the graphs, good approximations for both 900 MHz and 1800 MHz are achieved. Comparisons between Optimized model and picocell propagation models for different scenarios are shown in Table 4.4, Table 4.5, Table 4.6, Table 4.7 and Table 4.8.

Table 4.4. Comparison of models for single-floor cases.

Model	Mean Error (900 MHz)	Mean Error (1800 MHz)
Single-Slope	5.8	5.4
Dual-Slope	10.2	11.0
ITU-R Model	7.7	7.0
Motley-Keenan	5.9	5.7
Improved Motley-Keenan	4.2	4.9
Akerberg	7.8	7.3
Multi-Wall	4.1	5.2
Winner II	-	6.5
Lecours	5.0	-
UTD Indoor	4.9	-
Optimized	3.2	4.3

Table 4.5. Comparison of models for multi-floor cases.

Model	Mean Error (900 MHz)	Mean Error (1800 MHz)
Single-Slope	9.2	8.9
Dual-Slope	44.3	43.8
ITU-R	14.6	13.9
Motley-Keenan	5.0	7.2
Improved Motley-Keenan	4.3	6.8
Akerberg	36.2	35.2
Multi-Wall	5.0	3.4
Winner II	-	15.1
Lecours	4.5	-
UTD Indoor	4.4	-
Optimized	4.1	5.1

Table 4.6. Comparison of models for LOS cases.

Model	Mean Error (900 MHz)	Mean Error (1800 MHz)
Single-Slope	4.3	3.1
Dual-Slope	2.7	3.2
ITU-R	12.5	11.2
Motley-Keenan	2.7	4.0
Improved Motley-Keenan	2.7	4.0
Akerberg	9.5	8.5
Multi-Wall	3.5	3.2
Winner II	-	5.7
Lecours	2.5	-
UTD Indoor	2.2	-
Optimized	2.4	3.0

Table 4.7. Comparison of models for light obstruction cases.

Model	Mean Error (900 MHz)	Mean Error (1800 MHz)
Single-Slope	8.4	6.5
Dual-Slope	6.3	10.9
ITU-R	6.8	3.7
Motley-Keenan	8.2	5.9
Improved Motley-Keenan	5.9	8.5
Akerberg	7.0	6.2
Multi-Wall	4.0	8.4
Winner II	-	6.2
Lecours	5.7	-
UTD Indoor	3.5	-
Optimized	3.5	5.1

Table 4.8. Comparison of models for heavy obstruction cases.

Model	Mean Error (900 MHz)	Mean Error (1800 MHz)
Single-Slope	5.6	6.1
Dual-Slope	14.5	14.2
ITU-R	5.9	6.2
Motley-Keenan	6.6	6.4
Improved Motley-Keenan	4.3	4.2
Akerberg	7.3	7.1
Multi-Wall	4.4	5.1
Winner II	-	6.9
Lecours	5.8	-
UTD Indoor	6.5	-
Optimized	3.4	4.6

For single-floor case with all scenarios included, Optimized model proved to be

the best model with small improvements over Improved Motley-Keenan model and Multi-Wall model at both 900 MHz and 1800 MHz. For multi-floor case, it has the same performance with Multi-Wall model. For LOS propagation scenarios, Optimized model gave the best results with parameter optimization and the addition of second-slope. For lightly-obstructed scenarios, no improvement is achieved but close results to best models in terms of light obstruction cases are accomplished. Marginal improvement is achieved for heavily-obstructed cases at 900 MHz and the same results are obtained for 1800 MHz.

In summary, Optimized model presented most accurate predictions in our office environment by combining wall attenuation model of Improved Motley-Keenan model, second-slope of Dual-Slope model, diffraction and angle of incidence approach of UTD indoor model, traversing effect of Multi-Wall-and-Floor Model and Blaunstein's waveguide corridor model. Blaunstein's model could not be tested in our environment as it did not include any sufficiently long corridors that would justify the conditions of the model. It is still included in the proposed Optimized model so as to present a complete model that would fit to different office environments as well.

5. CONCLUSION

This thesis outlines indoor propagation models for frequencies of GSM band. The trend in mobile communication is to reduce base station cell sizes to single buildings and to even a single floor due to ever increasing bandwidth need. Estimating signal strength is critical for picocell deployment because low signal strength could mean gaps in the coverage while excessively high signal levels may risk going over electromagnetic exposure rules. Because of this need, it is important to have accurate indoor propagation models. Thus, this thesis aims to search accuracy of existing indoor propagation models and to derive an efficient and quick method optimized for an office environment.

This dissertation starts with explaining mobile communication channel and major propagation factors affecting it. Then it proceeds with existing indoor propagation models in the literature. Each model is explained in detail and their respective formulas are presented.

In order to test the existing indoor propagation models, measurements were taken at an office building. Each measurement location was marked on the map. Thicknesses and losses of walls were measured. Then models are implemented to each measurement scenario. Predictions of the models are then compared to actual measurement results. Performance of each model are compared with their absolute mean errors.

It has been observed that addition of several wall types and thickness information into propagation formula significantly improve the accuracy of the models. Different path loss patterns in the near zone of the antenna were observed during measurements. Effects like diffraction, traversing and angle of incidence were also observed to make positive contributions in measurement cases that suit them.

Using the performances of the existing models as a base, this thesis suggests a model optimized for an office environment. Factors working well in the existing models were used in the optimized model. Input parameters were also revised to obtain best

predictions. As a result, a model with better performance was obtained.

This thesis' main contribution is the derivation of an office-optimized indoor propagation model. The model is quick and easy to use and gave good predictions in our measurement site. Once a site-map is obtained, the model could be used to make quick signal level estimations. Multi-wall effects, wall thickness effects, floor attenuation, diffraction, traversing, angle of incidence and dual-slope effects are evaluated in the model. Some shortcomings of the model could be listed as; inability to account for metallic obstructions, especially high ones and lack of several floor measurements and unverified waveguiding feature. Optimized model is tested for only 900 MHz and 1800 Mhz and at only one place. Testing of the model at different frequencies and in another environment could be a future work.

REFERENCES

1. Meurling, J. and R. Jeans, *The Mobile Phone Book*, Communications Week International, London, 1994.

2. Rappaport, T. S., *Wireless Communications: Principles and Practice*, Prentice Hall, Englewood Cliffs, NJ, 2001.

3. Molisch, A. F., *Wireless Communications, 2nd Edition*, John Wiley, Los Angeles, USA, 2010.

4. Saunders, S. R. and A. A. Zavala, *Antennas and Propagation for Wireless Communication Systems, 2nd Edition*, John Wiley, Surrey, 2007.

5. Haslett, C., *Essentials of Radio Wave Propagation*, Cambridge University Press, Ofcom, UK, 2008.

6. Heavens, O. S., *Optical Properties of Thin Solid Films*, Dover Publications, New York, USA, 1965.

7. Cheng, D. K., *Field and Wave Electromagnetics*, 2nd ed., Addison-Wesley, Chevy Chase, Maryland, 1989.

8. COST231 final report, COST Action 231, *Digital Mobile Radio Towards Future Generation Systems*, European Commission/COST Telecommunications, Brussels, Belgium, 1999.

9. Lahteenmaki, J., "Indoor propagation between floors at 855 MHz and 1.8 GHz", COST 231, 1994.

10. Solahuddin, Y. F. and R. Mardeni, "Indoor empirical path loss prediction model for 2.4 GHz 802.11n network", *IEEE International Conference on Control System, Computing and Engineering*, pp. 12–17, 2011.

11. Sarkar, T. K., Z. Ji, K. Kim, A. Medouri and M. Salazar-Palma, "A survey of various propagation models for mobile communication", *IEEE Antennas and Propagation Magazine*, Vol. 45, No. 3, pp. 51–82, 2003.

12. Seidel, S. and T. Rappaport, "914 MHz path loss prediction models for indoor wireless communications in multifloored buildings", *IEEE Transactions on Antennas and Propagation*, Vol. 40, No. 2, pp. 207–217, 1992.

13. ITU-R Recommendation P.1238, *Propagation data and prediction models for the planning of indoor radio communication systems and radio local area networks in the frequency range*, International Telecommunication Union, Geneva, 1997.

14. Motley, A. J. and J. M. P. Keenan, "Personal communication radio coverage in buildings at 900 MHz and 1700 MHz", *Electronics Letters*, Vol. 24, No. 12, pp. 763–764, 1988.

15. Lima, A. G. M. and L. F. Menezes, "Motley-Keenan model adjusted to the thickness of the wall", *International Conference on Microwave and Optoelectronics*, pp. 180–182, 2005.

16. Akerberg, D., "Properties of a TDMA pico cellular office communication system", *IEEE 39th Vehicular Technology Conference*, Vol. 1, pp. 186–191, 1989.

17. Lott, M. and I. Forkel, "A multi-wall-and-floor model for indoor radio propagation", *IEEE VTS 53rd Vehicular Technology Conference*, Vol. 1, pp. 464–468, 2001.

18. IST-4-027756, *WINNER II Channel Models*, Winner Information Society Technologies, 2008.

19. LaFortune, J.-F. and M. Lecours, "Measurement and modeling of propagation losses in a building at 900 MHz", *IEEE Transactions on Vehicular Technology*, Vol. 39, No. 2, pp. 101–108, 1990.

20. Cheung, K., J. H. M. Sau and R. Murch, "A new empirical model for indoor

propagation prediction", *IEEE Transactions on Vehicular Technology*, Vol. 47, No. 3, pp. 996–1001, 1998.

21. Kouyoumjian, R. G. and P. H. Pathak, "A uniform geometrical theory of diffraction for an edge in a perfectly conducting surface", *Proceedings of the IEEE*, Vol. 62, No. 11, pp. 1448–1461, 1974.

22. Pena, D., R. Feick, H. Hristov and W. Grote, "Measurement and modeling of propagation losses in brick and concrete walls for the 900-MHz band", *IEEE Transactions on Antennas and Propagation*, Vol. 51, No. 1, pp. 31–39, 2003.

23. Stone, W. C., "Electromagnetic Signal Attenuation in Construction Materials", NIST Construction Automation Program Report No. 3, 1997.

24. Micheli, D., A. Delfini, F. Santoni, F. Volpini and M. Marchetti, "Measurement of electromagnetic field attenuation by building walls in the mobile phone and satellite navigation frequency bands", *IEEE Antennas and Wireless Propagation Letters*, Vol. 3, pp. 15–20, 2014.

25. Seker, S., A. Tesneli and O. Cerezci, "UHF ray tracing propagation model for corridors", *IEEE International Symposium on Electromagnetic Compatibility*, Vol. 1, pp. 657–659, 2003.

26. Luebbers, R., "Finite conductivity uniform GTD versus knife edge diffraction in prediction of propagation path loss", *IEEE Transactions on Antennas and Propagation*, Vol. 32, No. 1, pp. 70–76, 1984.

27. El-Sallabi, H., G. Liang, H. L. Bertoni, I. Rekanos and P. Vainikainen, "Influence of diffraction coefficient and corner shape on ray prediction of power and delay spread in urban microcells", *IEEE Transactions on Antennas and Propagation*, Vol. 50, No. 5, pp. 703–712, 2002.

28. Seker, S. and G. Apaydin, "New Physical Discrete UHF Multilayer Propagation

Model for Urban Areas", *ACES Journal*, Vol. 23, pp. 126–133, 2008.

29. Blaunstein, N., "Average field attenuation in the nonregular impedance street waveguide", *IEEE Transactions on Antennas and Propagation*, Vol. 46, No. 12, pp. 1782–1789, 1998.